The shape of the outer-Galaxy HI layer. I - Atlas of volume densities in cuts through a composite, galactocentric data cube

Burton, W.B.; te Lintel Hekkert, P.

ASTRONOMY & ASTROPHYSICS
SUPPLEMENT SERIES

SEPTEMBER **1986,** PAGE 427

Astron. Astrophys. Suppl. Ser. **65,** 427-463 (1986)

The shape of the outer-Galaxy HI layer. I. Atlas of volume densities in cuts through a composite, galactocentric data cube

W. B. Burton and P. te Lintel Hekkert

Sterrewacht Leiden, P.O. Box 9513, 2300 RA Leiden, The Netherlands

Received August 22, accepted December 9, 1985

Summary. — Presented here are cuts through a composite galactocentric data cube which form the observational foundation for a quantitative investigation of the warped and flaring outer parts of the hydrogen layer in our Galaxy. Much of the material in the data cube comes from the Leiden-Green Bank HI survey of Burton (1985) and Burton and te Lintel Hekkert (1985). To give the highest possible density of coverage we combined that material with the more densely sampled data of Westerhout and Wendlandt (1982), Weaver and Williams (1973), and Burton and Liszt (1983). The southern part of the sky at $\delta < -46^\circ$ is represented by the Parkes data of Kerr *et al.* (1986). In l, b, v coordinates the composite data cube covers 360° of l, a range of b extending from at least $\pm 10^\circ$ in parts of the southern sky to $-20^\circ \leq b \leq 33^\circ$ over much of the northern sky, and a range of velocities covering essentially all of the emission from the Galaxy. This cube was transformed from brightness temperatures in an array of heliocentric coordinates l, b, v to HI volume densities in an array of galactocentric cylindrical coordinates R, θ, z using the v-to-R conversion consistent with a flat rotation curve with $\theta(R > R_0 = 10 \text{ kpc}) = 250 \text{ km s}^{-1}$. The volume densities are shown in an atlas of cuts through the galactocentric data cube at constant R-values in θ, z coordinates, at constant θ-values in R, z coordinates, and at constant z-values in R, θ coordinates. Shown in addition are maps of the galactic arrangement in R, θ coordinates of projected HI surface densities, z-height of the gas-layer centroid, maximum volume density, z-height of the location of maximum volume density, as well as measures of the layer thickness ; these additional maps are shown both for the case of a flat rotation curve determining the v-to-R conversion as well as for the case of an axisymmetric, rising outer-Galaxy rotation curve. The interpretative analysis of the material is the subject of two additional papers in this series.

Key words : Atlases — Galaxy (the) : kinematics and dynamics of — Galaxy (the) : structure of — interstellar medium : kinematics and dynamics of — radio lines : 21-cm.

1. Introduction.

It has been known since the early 21-cm surveys became available that the layer of atomic hydrogen in the outer parts of the Milky Way is systematically warped from the galactic equator defined by the plane $b = 0^\circ$ (Burke, 1957 ; Kerr, 1957 ; Westerhout, 1957 ; Oort *et al.*, 1958). Motivation for a thorough investigation of the shape of the gas layer in the Milky Way is provided by the accumulated evidence showing that large-scale deviations of the HI from a flat disk are common for spiral galaxies — although the dynamical mechanism is not yet understood — and by the realization that the substantial dark component of the galactic potential can be traced effectively by study of the motions and form of the outer-Galaxy HI layer.

There have been three principal obstacles to quantitative improvement of the description of the HI gas layer in the outskirts of the Milky Way. The first of these obstacles involved the lack, until recently, of adequate observational coverage of the part of the Milky Way only visible from the southern hemisphere. The data taken with the Parkes 60-foot telescope by Kerr *et al.* (1986) effectively completed the coverage established by Weaver and Williams (1973) between $-10^\circ \leq b \leq 10^\circ$ to include all longitudes. The analysis by Henderson *et al.* (1982) made use of the combined northern and southern $|b| \leq 10^\circ$ data and was thus the first to produce a global description of any detail of the warped gas layer.

The second of the obstacles involved the uncertainties in the outer-Galaxy distance scale. Evidence that external spiral galaxies with the same general morphology as the Milky Way have rotation curves which remain flat, or even rise, well beyond their optical limits suggested that the falling curve used in early investigations of the outer gas layer is not a realistic one. Henderson *et al.* (1982) based their description on the distance scale appropriate to a flat curve ; Kulkarni *et al.* (1982) reanalysed the Weaver and Williams data using the rising rotation curve found by Blitz *et al.* (1980) from CO velocities of HII regions with optically-determined distances. These two

studies provided new insights into the scale and form of the warped gas disk.

The third obstacle to a thorough description of the outer-Galaxy gas layer involves the constraints posed by the latitude coverage, and sensitivity, of the earlier data. The present investigation addresses this obstacle, by making use of the observations forming the Leiden-Green Bank Survey (Burton, 1985 ; Burton and te Lintel Hekkert, 1985). Although that survey represents an improvement over earlier data in terms of sensitivity, velocity resolution, velocity coverage, and extent of coverage, especially in latitude — it was not made with particularly detailed positional resolution, nor does it reach parts of the southern sky at $\delta < -46°$. Consequently the data cube used here combines the new with existing material in order to give the highest-possible density of coverage over as much of the galactic disk as possible.

2. Material comprising the composite observational data cube.

The material used in the composite data cube is summarized in table I. The columns tabulate, respectively, the appropriate reference for each survey, the telescope on which it was made, the coverage (at $b = 0°$) and the spacing in longitude, the coverage and spacing in latitude, the resolution Δv in velocity, the 3 σ sensitivity level in brightness temperatures, and a priority specifying which material was used at grid points represented in more than one survey. The Δv and 3 σ levels in parentheses in the table refer to values at low intensity levels obtained after smoothing in the manner described in the references given. The priority assigned favors the Leiden-Green Bank survey at grid points were it exists because of its low Δv and high sensitivity. The extent of the latitude coverage of this survey is particularly important in longitude quadrants I and II where the signature of the warped layer extends well beyond 10° latitude. At large distances from the Sun the one-degree spacing of the Leiden-Green Bank grid is coarser than desired for a detailed description of the properties of the layer : at 20 kpc distance, one degree subtends 350 pc. Consequently the more densely-sampled surveys were entered into the data cube at positions not observed in the Leiden-Green Bank work, with priority as given in table I. The Maryland-Parkes survey of Kerr *et al.* (1986), which was provided to us in advance of publication, is the only suitable material available for much of the southern sky and is therefore crucial to this work.

Each of the surveys entered in the composite contains intensities on the brightness temperature scale used by Williams (1973). In the atlas of maps presented here no important systematic difference in intensity occurs from one survey to another. The differing noise levels can be seen, for example, in the $\theta, z\,|_R$ maps at large values of R where the intensities measured in the gas layer are weak. At small R-values, where intensities are higher, the borders of the data cube are evident. Thus in the θ, z map at $R = 10.5$ kpc, the border at $\theta < 180°$, $z < 0$ kpc corresponds to the $b = -20°$ limit of the Leiden-Green Bank work, and the one at all θ values at $z > 0$ kpc to its upper limit at b varying between $+20°$ and $+33°$; the $\pm 10°$ latitude extent of the southern survey is evident in this map, as is, in the patch centred near $\theta = 260°$, $z = 3$ kpc, the region of the sky below the $\delta = -46°$ limit of the Leiden-Green Bank survey, but above the $b = +10°$ limit of the Maryland-Parkes work.

The number of significant bits of information in the composite T_b, l, b, v dataset, accounting for the number of grid points, the velocity extent and resolution, and the dynamic range in intensities, is about 10^{10}.

3. Converting the data cube from heliocentric to galactocentric coordinates.

Radial velocities measured in the outer Galaxy correspond to galactocentric distances in a single-valued manner under plausible assumptions of galactic kinematics. We carried out the v-to-R conversion for two assumed rotation curves, producing in fact two galactocentric data cubes. Most of the maps in the atlas pertain to a flat rotation curve, at a value $\theta = 250$ km s^{-1} for distances greater than the solar distance, R_0, taken here as 10 kpc. We also carried out the conversion for the rising curve found observationally by Blitz *et al.* (1980), and expressed for $\theta_0 = 250$ km s^{-1} and $R_0 = 10$ kpc. Our principal results in the subsequent analysis are to be given for the case of a flat curve, as well as for a rising one.

A few comments on the v-to-R conversion are called for. The assumed rotation curves contain no small-scale irregularities of the sort which might be associated with a localized mass concentration and which might, for example, cause the v-to-R relationship to be locally multivalued. We know too little of the details of mass distribution to be able to account for such a possibility in a realistic way. In any case, the global properties of the gas layer are probably little affected. Potentially more important is the cylindrical kinematic symmetry imposed by use of the same rotation curve for all galactocentric azimuths. It has long been known that the velocity range of gas near the galactic equator is systematically larger at southern longitudes than the complementary northern ones (see e.g. Fig. 4.7 in Burton, 1974 and Shuter, 1982). As is so often the case in interpreting galactic HI data, one must decide if the profile structure in question is a consequence of the spatial distribution of the gas or of its kinematics. Although work on the southern outer-Galaxy rotation curve is currently not yet in a definitive state, the work of Brand *et al.* (1985) shows that the general southern curve is flat, or rising, as in the north : in order for the north, south velocity-range asymmetries to be solely kinematic in origin the southern curve would have to fall at $R > R_0$, and this is ruled out by the work of Brand *et al.* It seems not unlikely that our Galaxy is lopsided in the sense demonstrated by Baldwin *et al.* (1980) for a number of nearby systems. In the interpretation articles to follow we comment further on the plausibility and consequences of the imposed kinematic symmetry.

The measured intensities have been corrected for optical depth in the simplest possible way, assuming a uniform HI spin temperature, $T_s = 130$ K. The HI

column density (see Kerr, 1968) is given by $N_{HI} = 1.823 \times 10^{18} \int T_s \tau(\nu)\, d\nu$ cm^{-2}, where $\tau(\nu) = -\ln\left(1 - T_b(\nu)/T_s\right)$. N_{HI} is in general not a measured quantity. In the case of a profile optically thin at all velocities N_{HI} is measurable through the profile integral $\int T_b(\nu)\, d\nu$ because in this case $T_b(\nu) \approx T_s \tau(\nu)$. The volume density smoothed over a length Δr pc is then $n_{HI} = 0.59 \int T_b\, d\nu/\Delta r$ cm^{-3}. Although consequences of finite optical depth are no doubt generally less severe in the outer Galaxy than in the inner, $\tau \geqslant 1$ probably pertains within $\pm 20°$ of the center and anticenter directions. For significantly large optical depth, the integral measure $\int T_b\, d\nu/\Delta r$ approaches $T_s \left|\frac{\Delta\nu}{\Delta r}\right|$. Thus both in the thin case as well as in the thick one, the arrangement of the geometrical kinematic parameter largely determines the manner in which the HI gas layer is perceived in the observations.

The behaviour of the kinematic parameter $\left|\frac{d\nu}{dr}\right|$ determines the basic appearance and degree of saturation along individual lines of sight. The influence of the parameter is most readily followed in the observer-centred coordinate l, b, ν system. Although its influence in galactocentric coordinates is pervasive at $R < R_0$, at $R > R_0$ its influence is rather straightforward. A plot of the galactic distribution of the parameter is given in figure 1, for the case of the flat rotation curve ; the kinematic behaviour is schematically similar for other simple rotation fields. At $R > R_0$, $\left|\frac{d\nu}{dr}\right|$ is near zero in two wedges, centred on $\theta = 0°$ and $\theta = 180°$. Viewed from the galactic center, the wedge at $\theta = 0°$ is wider than the one at $\theta = 180°$; both wedges increase in width as R increases. Thus the resolution in velocity is poor near $\theta = 0°$ and 180°, and becomes increasingly worse in these directions as R increases. The R, θ maps show bands in these directions which represent systematic errors due to the resolution in velocity described by the $\left|\frac{d\nu}{dr}\right|$ parameter. Data referring to within about 15° of $\theta = 180°$, and within about 20° of $\theta = 0°$ should be regarded with caution. Outside these azimuth wedges, the influence of the velocity-crowding parameter is fortunately both small and uniform at $R > R_0$. It is important in this regard that the velocity dispersion characterizing galactic HI profiles is evidently quite constant ($\leqslant 10$ km s^{-1}) over most of the Galaxy : systematic variations in the dispersion, for example with R, would be reflected in the form of the influence of the $\left|\frac{d\nu}{dr}\right|$ parameter.

The galactocentric, cylindrical-coordinate, R, θ, z data cube contains HI volume density information at 1°-spacings in θ, and at intervals of 250 pc in R and of 100 pc in z. The atlas which follows shows cuts along each of the three coordinates of the cube corresponding to the flat-rotation-curve ν-to-R conversion.

The different parts of figure 2 show in $\theta, z\,|_R$ maps the distribution of average hydrogen volume densities in cylinders with 250 pc thick walls centred at the indicated distances R. The panels of figure 3 show in $R, z\,|_\theta$ maps the distribution of average volume densities in sheets perpendicular to the galactic equator running through the galactic center at the indicated azimuth θ. The panels of figure 4 show in $R, \theta\,|_z$ maps the distribution of average volume densities in 100 pc thick sheets parallel to the galactic equator at the indicated z-heights.

The panels of figure 5 show some derived quantities specifying the shape of the outer-Galaxy HI layer. The upper panels in figure 5 refer to the data cube based on a flat rotation curve ν-to-R conversion ; the lower panels refer to the data cube based on the rising rotation curve of Blitz *et al.* (1980). For emission observed along a particular line of sight, the changes to distance corresponding to a change from a flat to a rising curve involve a rather straightforward scaling, but this is not the case in the R, θ, z cube.

Shown in the panels of figure 5 are, respectively, the value of the projected HI surface density, the z-height of the mass centroid of the HI density, the value of the maximum volume density, the z-height of the maximum volume density, the thickness of the hydrogen layer containing half the total surface density as measured between z-heights at which the surface density is one-quarter of the total surface density projected over all z, and the thickness of the layer measured between z-heights where the total volume density is half of the maximum value.

The astrophysical interpretation of this material is the subject of two following papers.

Acknowledgements.

We are grateful to F. J. Kerr, P. F. Bowers, P. D. Jackson and M. Kerr for sharing their Parkes material with us before publication, and particularly to Dr. Jackson for preparing an export tape of the data for us. The extensive photographic work essential to this project was carried out by the Leiden Observatory photographer, W. Brokaar.

References

BALDWIN, J. E., LYNDEN-BELL, D., SANCISI, R. : 1980, *Mon. Not. R. Astron. Soc.* **193,** 313.
BLITZ, L., FICH, M., STARK, A. A. : 1980, *Proc. I.A.U. Symposium* **87,** 213.
BRAND, J., BLITZ, L., WOUTERLOOT, J. : 1985, *Mitt. Astron. Ges.* **63,** 207.
BURKE, B. F. : 1957, *Astron. J.* **62,** 90.
BURTON, W. B. : 1984, in *Galactic and Extragalactic Radio Astronomy,* K. I. Kellermann and G. L. Verschuur eds. (Springer-Verlag) p. 82.
BURTON, W. B. : 1985, *Astron. Astrophys. Suppl. Ser.* **62,** 365.
BURTON, W. B., TE LINTEL HEKKERT, P. : 1985, *Astron. Astrophys. Suppl. Ser.* **62,** 645.
BURTON, W. B., LISZT, H. S. : 1983, *Astron. Astrophys. Suppl. Ser.* **52,** 63.
HENDERSON, A. P., JACKSON, P. D., KERR, F. J. : 1982, *Astrophys. J.* **263,** 116.
KERR, F. J. : 1957, *Astron. J.* **62,** 93.
KERR, F. J. : 1968, in *Stars and Stellar Systems*, Vol. 7, B. M. Middlehurst and L. H. Aller eds., Chicago, 574.
KERR, F. J., BOWERS, P. F., JACKSON, P. D., KERR, M. : 1986, *Astron. Astrophys. Suppl. Ser.,* in press.
KULKARNI, S. R., BLITZ, L., HEILES, C. : 1982, *Astrophys. J. Lett.* **259,** L63.
OORT, J. H., KERR, F. J., WESTERHOUT, G. : 1958, *Mon. Not. R. Astron. Soc.* **118,** 379.
SHUTER, W. L. H. : 1982, *Mon. Not. R. Astron. Soc.* **199,** 109.
WEAVER, H., WILLIAMS, D. R. W. : 1973, *Astron. Astrophys. Suppl. Ser.* **8,** 1.
WESTERHOUT, G. : 1957, *Bull. Astron. Inst. Neth.* **13,** 201.
WESTERHOUT, G., WENDLANDT, H.-U. : 1982, *Astron. Astrophys. Suppl. Ser.* **49,** 137.
WILLIAMS, D. R. W. : 1973, *Astron. Astrophys. Suppl. Ser.* **8,** 505.

TABLE I. — *Material combined in the galactic warp data cube.*

Reference	Telescope	ℓ-coverage	b-coverage	Δv	3σ sensitivity	Priority
Weaver and Williams (1973)	Hat Creek 85-foot	$10^{\circ} \leq \ell \leq 250^{\circ}$ $\Delta\ell = 0^{\circ}.5$	$\lvert b \rvert \leq 10^{\circ}$ $\Delta b = 0^{\circ}.25$	2.1 km s^{-1} (6.3)	1.7 K (1.0)	3
Westerhout and Wendlandt (1982)	NRAO 300-foot	$11^{\circ} \leq \ell \leq 235^{\circ}$ $\Delta\ell = 0^{\circ}.2$	$\lvert b \rvert \leq 2^{\circ}$ $\Delta b = 0^{\circ}.1$	2.0 km s^{-1}	2 K	2
Burton and Liszt (1983)	NRAO 140-foot	$349^{\circ} < \ell < 13^{\circ}$ $\Delta\ell = 0^{\circ}.5$	$\lvert b \rvert \leq 10^{\circ}$ $\Delta b = 0^{\circ}.5$	2.0 km s^{-1}	0.06 K	1
Kerr et al. (1986)	Parkes 60-foot	$240^{\circ} \leq \ell \leq 350^{\circ}$ $\Delta\ell = 0^{\circ}.5$	$\lvert b \rvert \leq 10^{\circ}$ $\Delta b = 0^{\circ}.25$	2.0 km s^{-1}	0.8 K	2
Burton (1985) and Burton and te Lintel Hekkert (1985)	NRAO 140-foot	$330^{\circ} \leq \ell \leq 270^{\circ}$ $\Delta\ell = 1^{\circ}.0$	$-20^{\circ} \leq b \leq 20^{\circ}$ (33°) $\Delta b = 1^{\circ}.0$	1.0 km s^{-1} (2.1)	0.2 K (0.1)	1

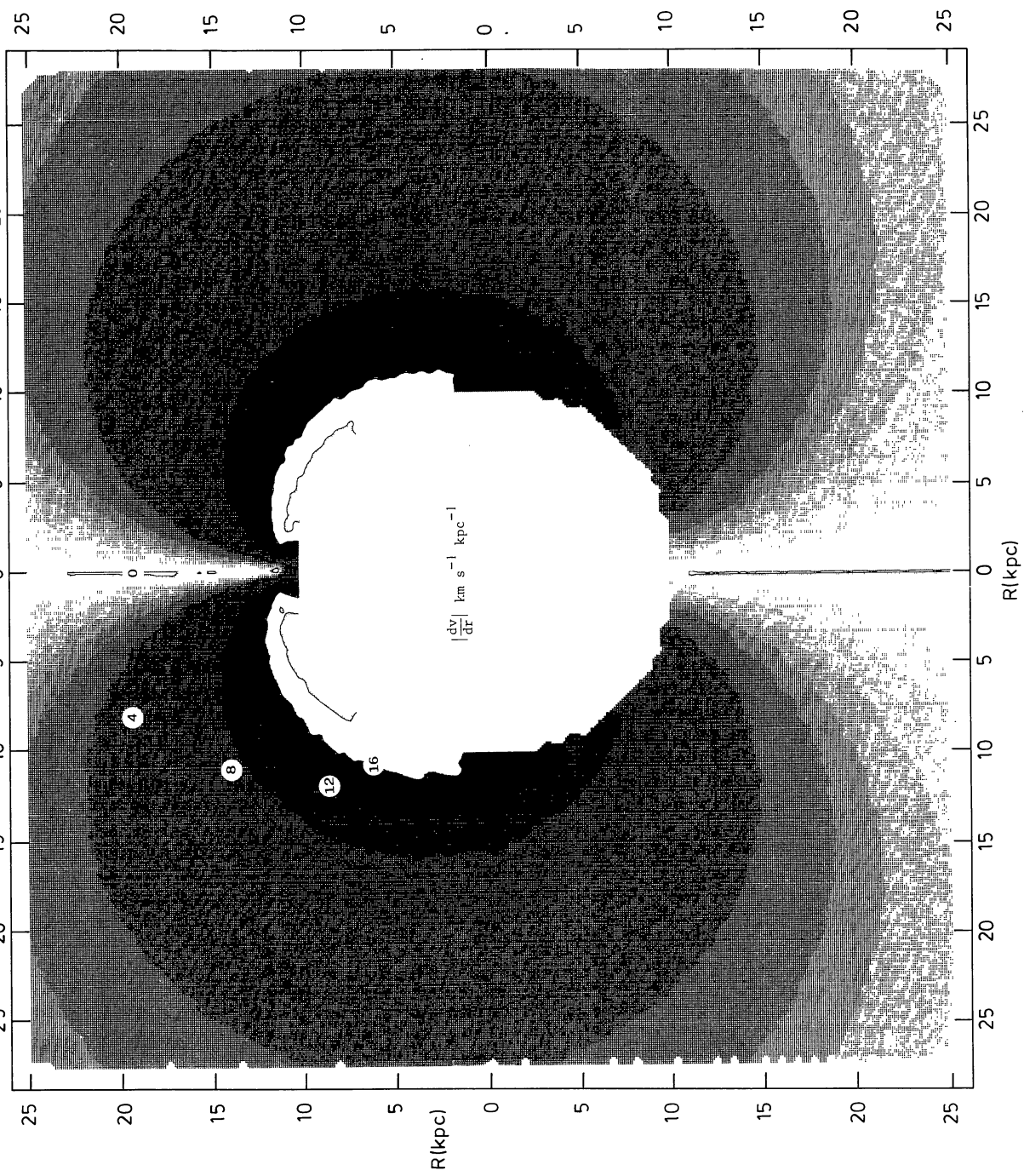

FIGURE 1. — Galactic distribution of the kinematic parameter $\left|\frac{dv}{dr}\right|$. The behaviour of this parameter along individual lines of sight determines important aspects of the observed 21-cm profiles. Except near $\theta = 0°$ and 180° the parameter fortunately has a rather smooth behaviour at $R > R_0$.

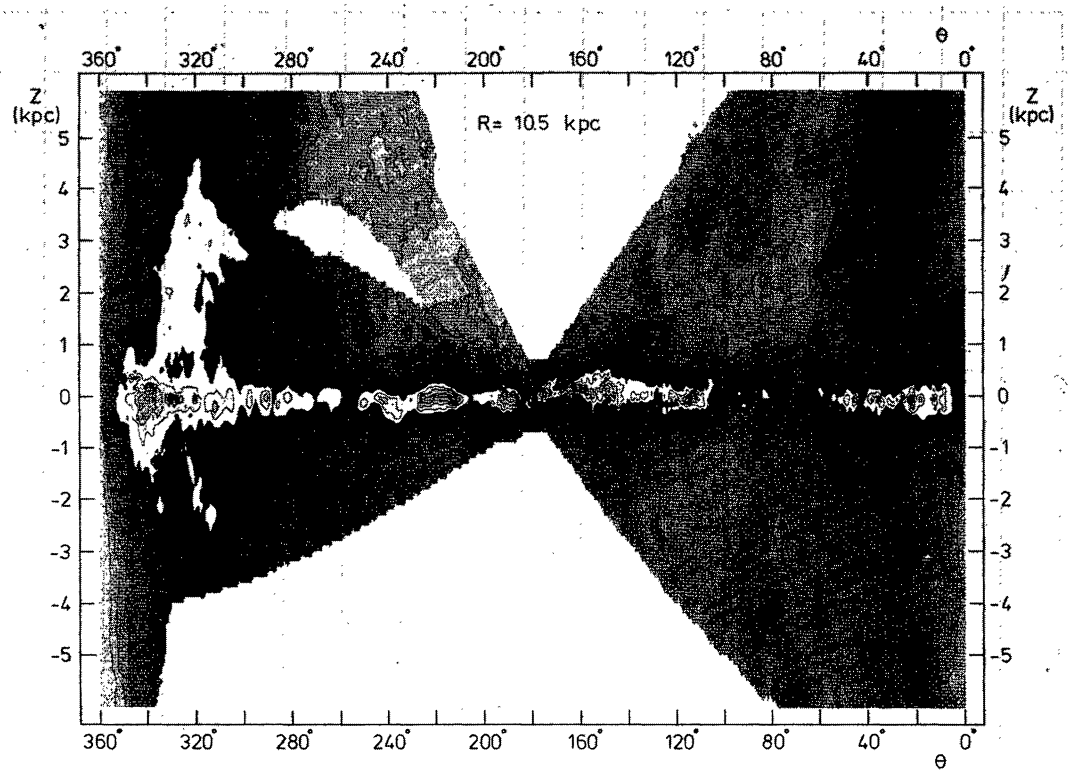

2(1)

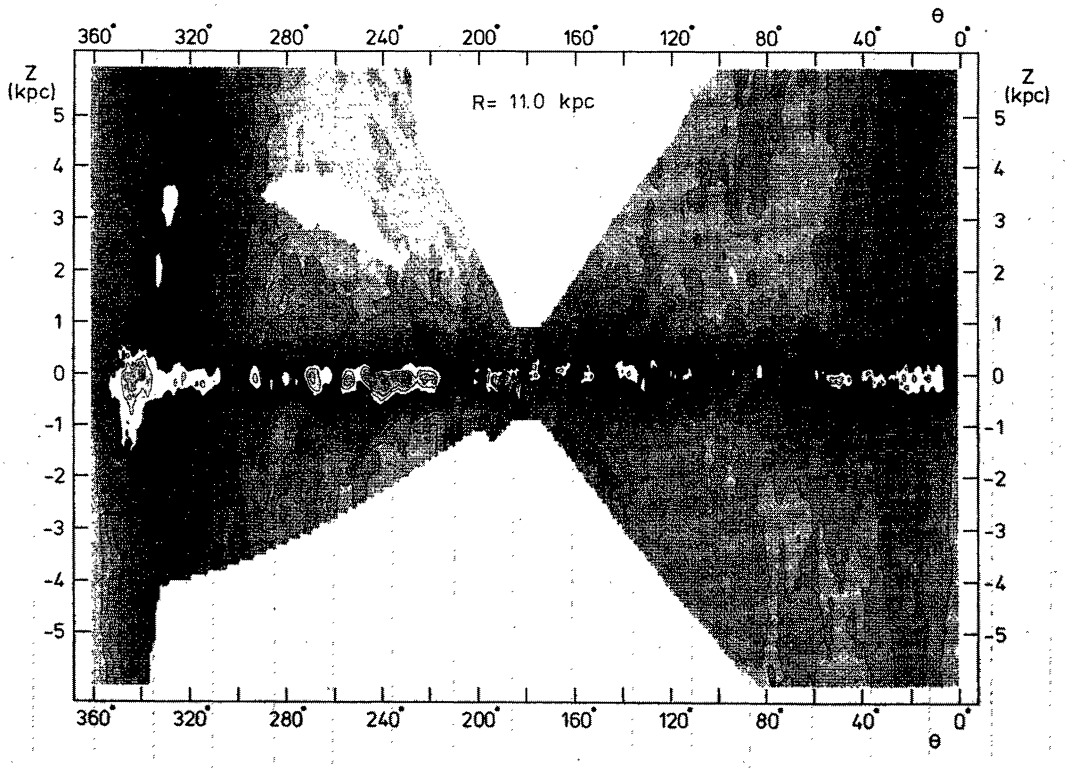

2(2)

FIGURES 2(1)-2(32). — $\theta, z\,|_R$ maps showing arrangement of hydrogen volume densities in cylinders with 500 pc thick walls centred at the indicated R. Contours are drawn at atoms per cubic centimeter levels of 0.01, 0.02, 0.03, 0.05, 0.07, 0.16, 0.30, 0.45, 0.6, 0.9, and 1.2. Grey scale divisions occur at levels of 0.001, 0.004, 0.01, 0.02, 0.03, 0.05, 0.07, 0.16, 0.30, 0.45, and 0.60 cm^{-3}. The darkest grey/white division occurs at densities $0.30 < n_{HI} < 0.45$ cm^{-3}; densities less than 0.001 cm^{-3} are coded white, as are unobserved regions. The cylindrical-coordinate R, θ, z data cube was sampled at 1° intervals in θ and 100-pc intervals in z.

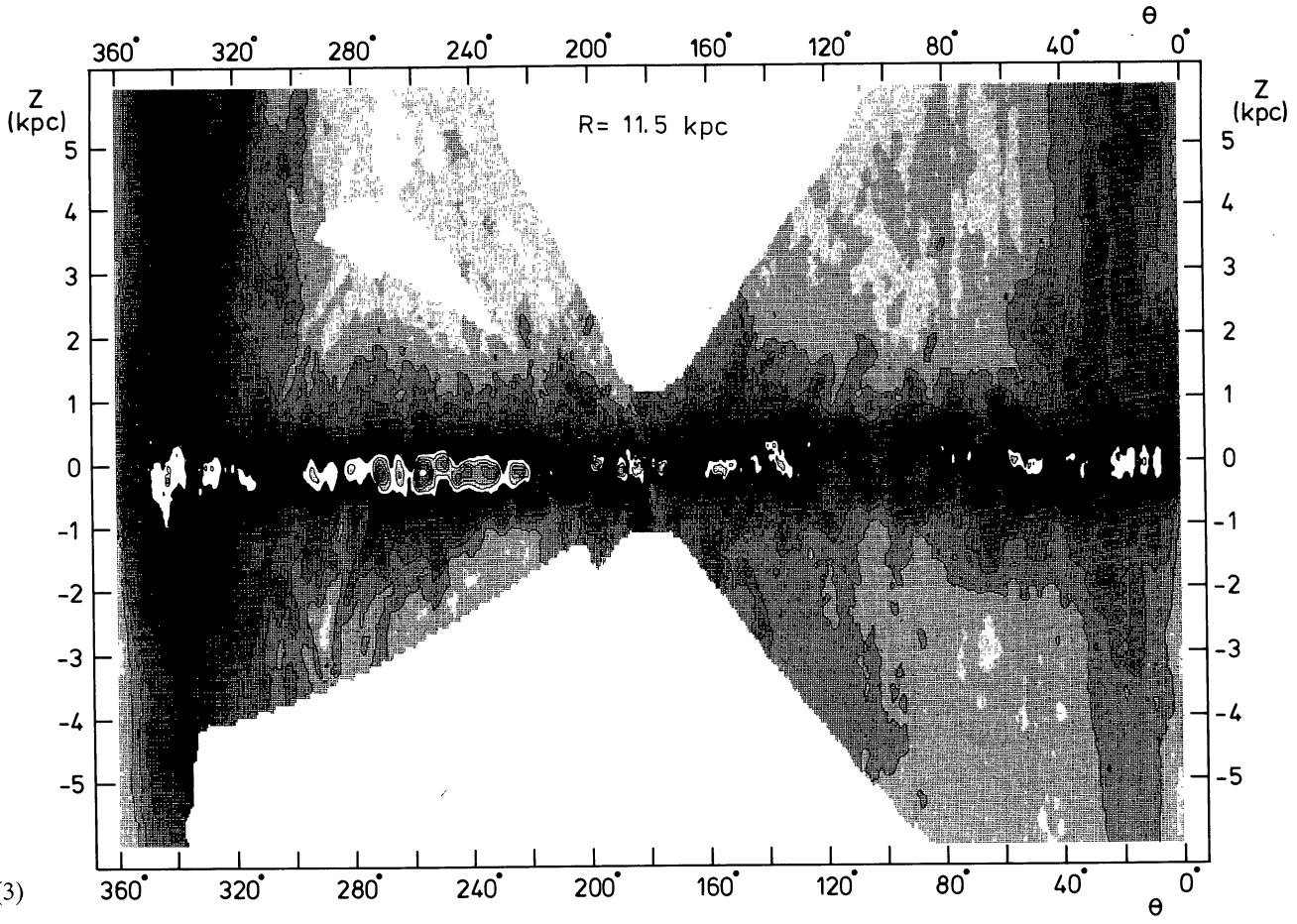

2(3)

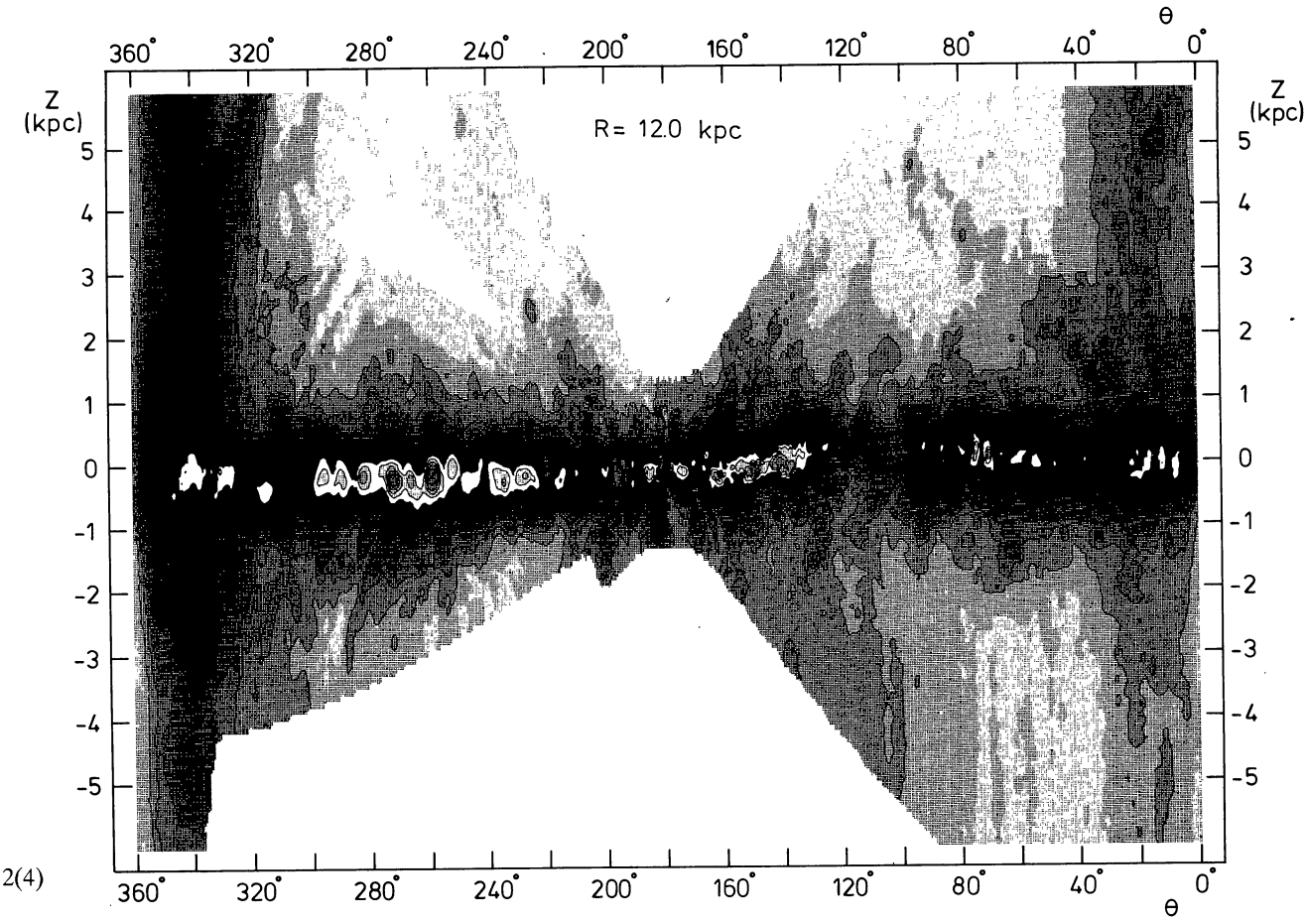

2(4)

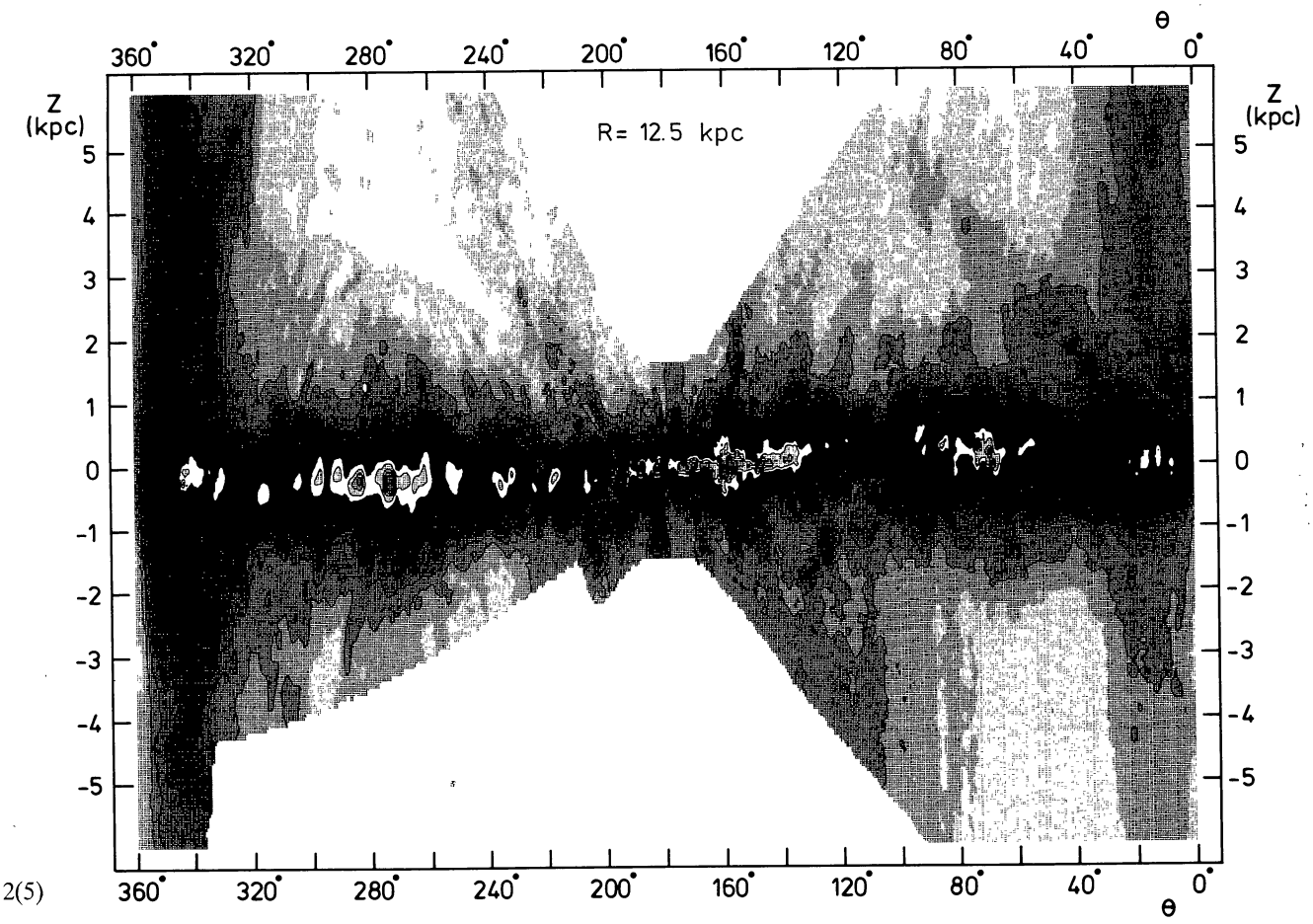

2(5)

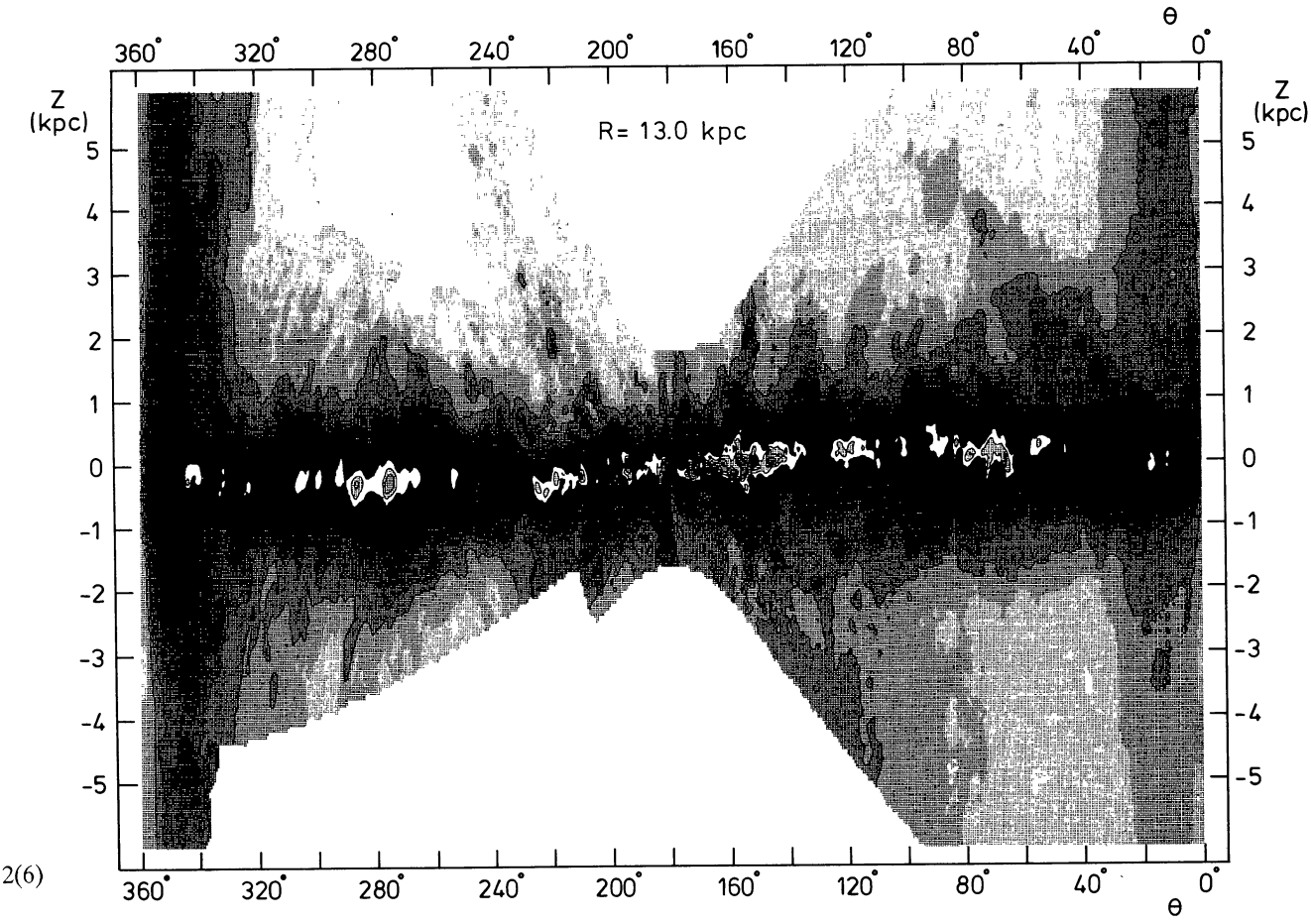

2(6)

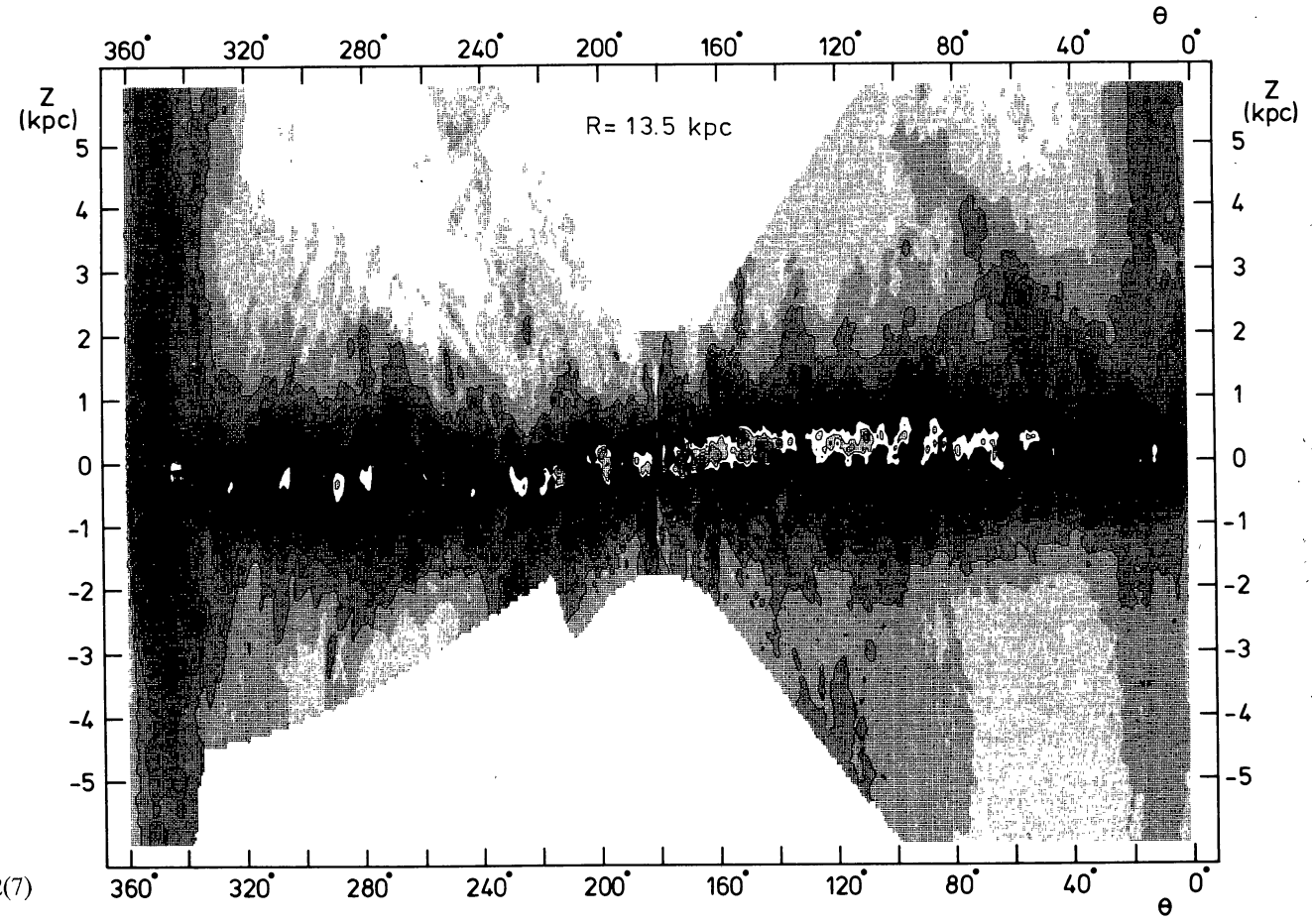

2(7)

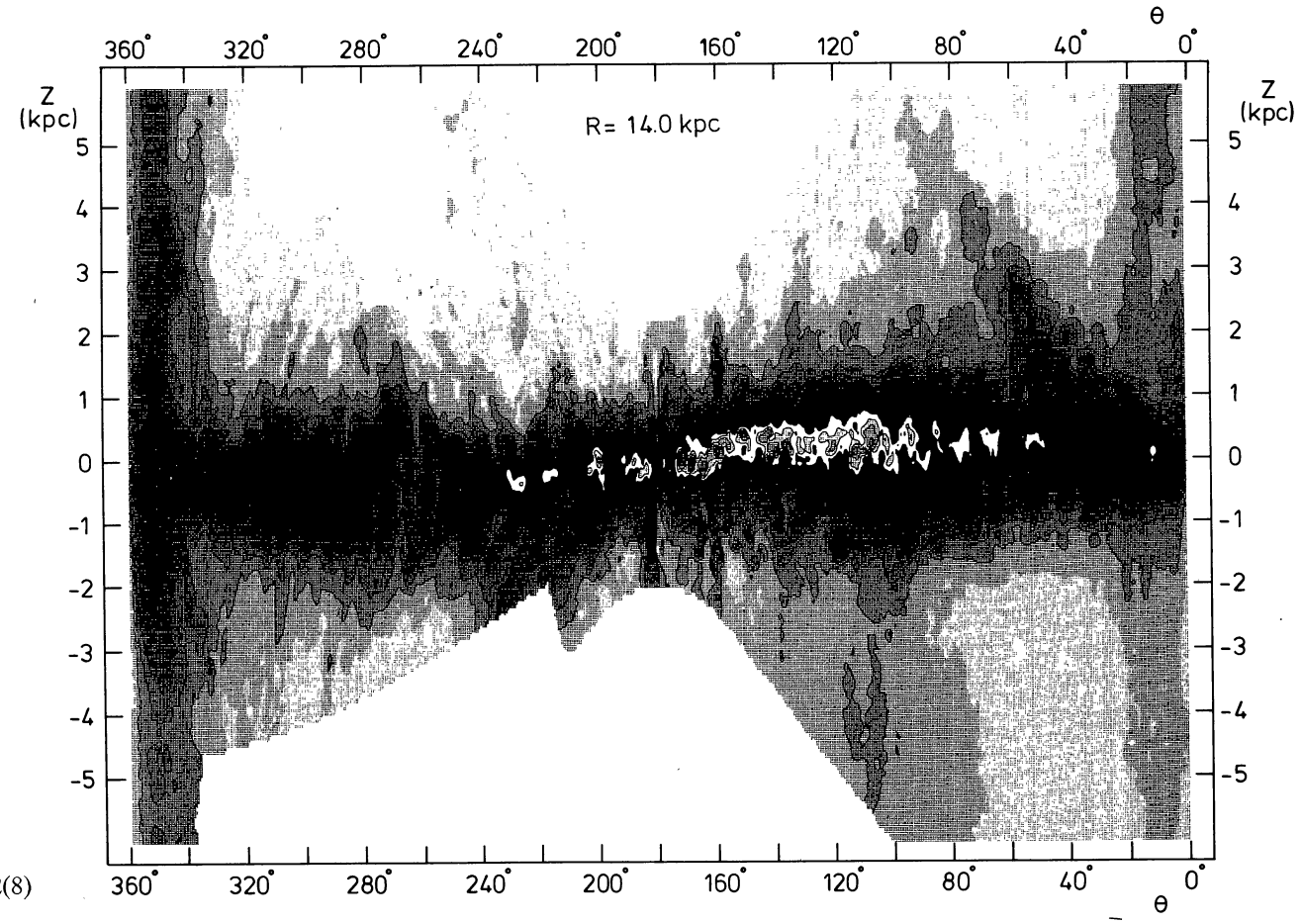

2(8)

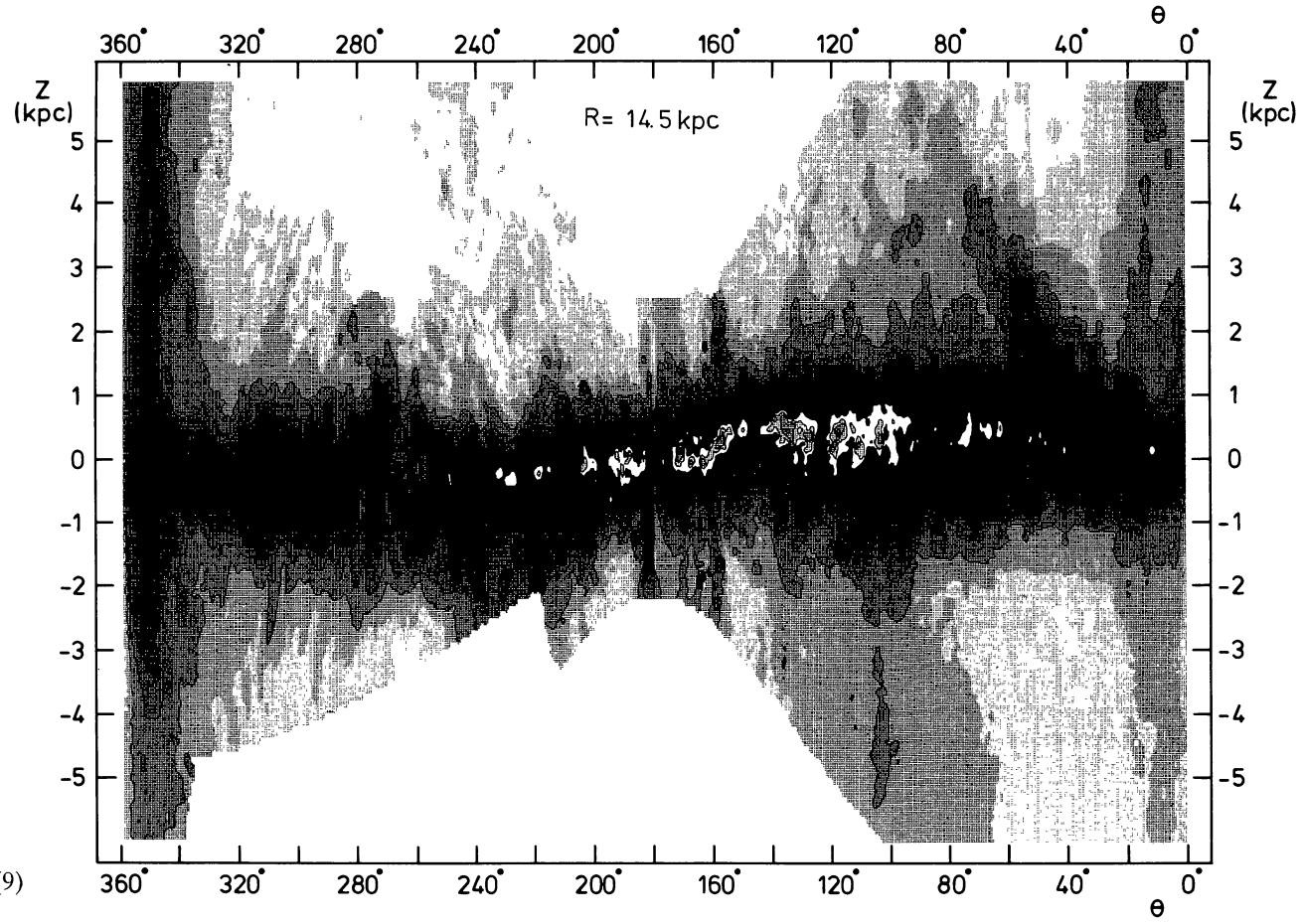

2(9)

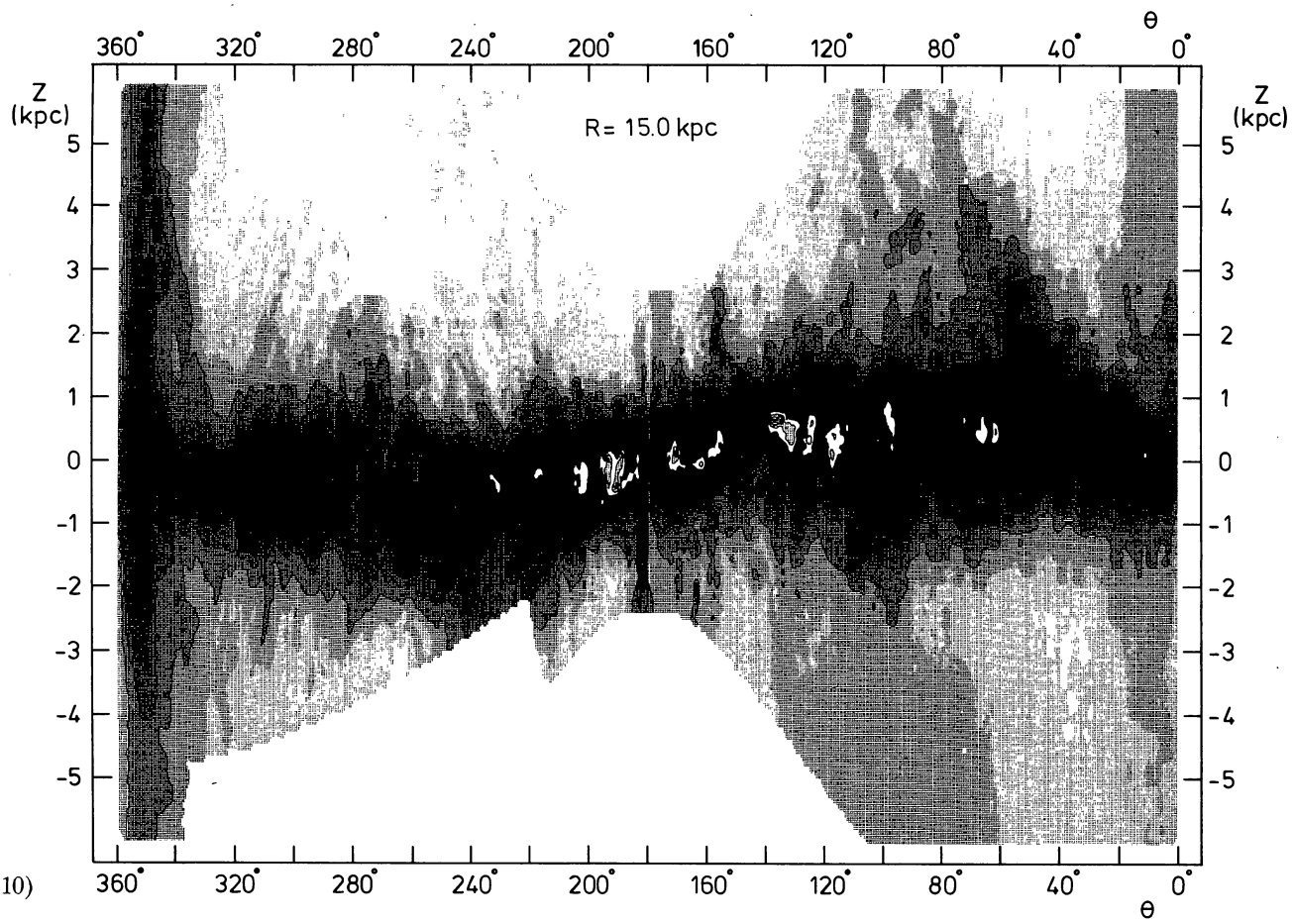

2(10)

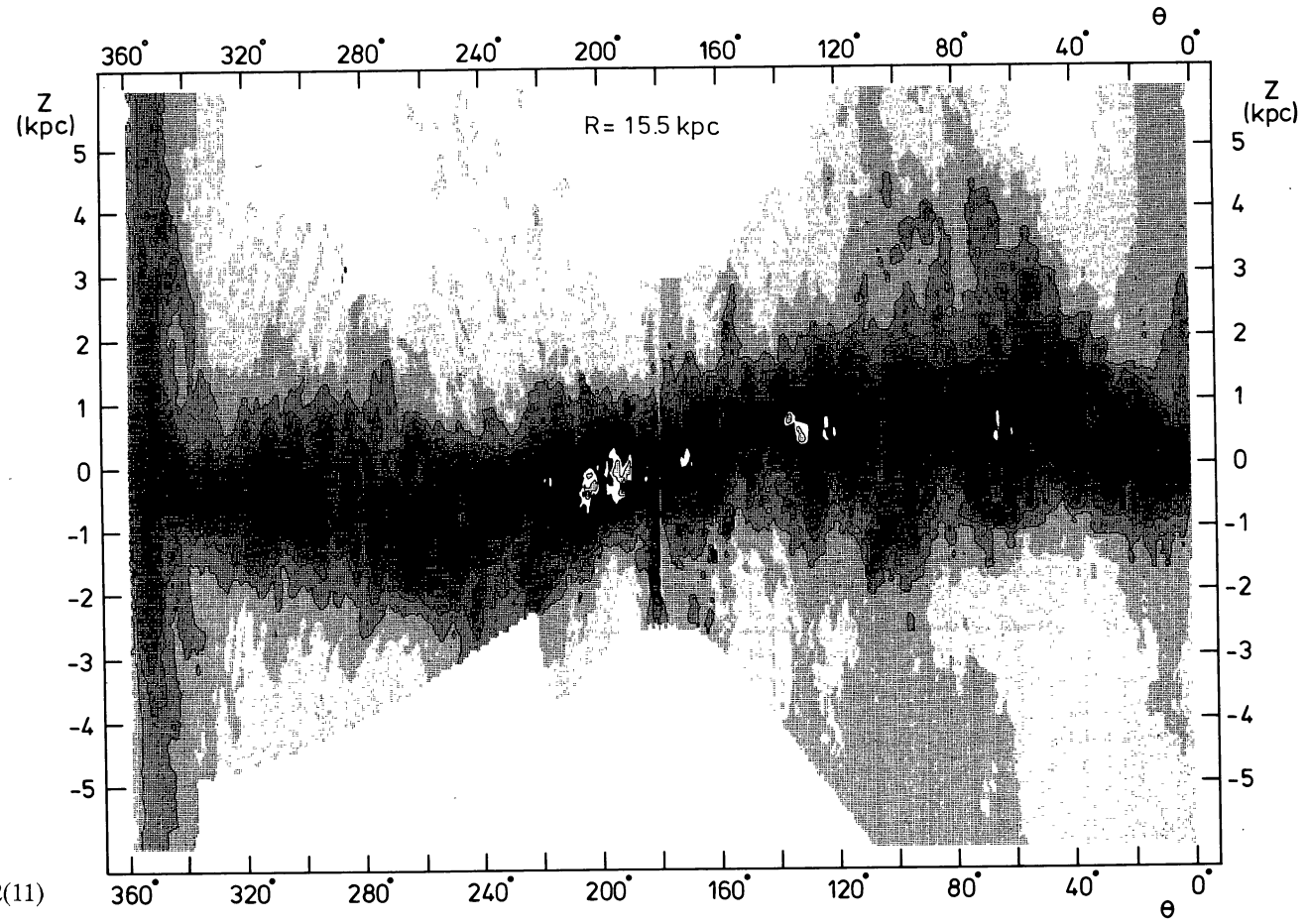

2(11)

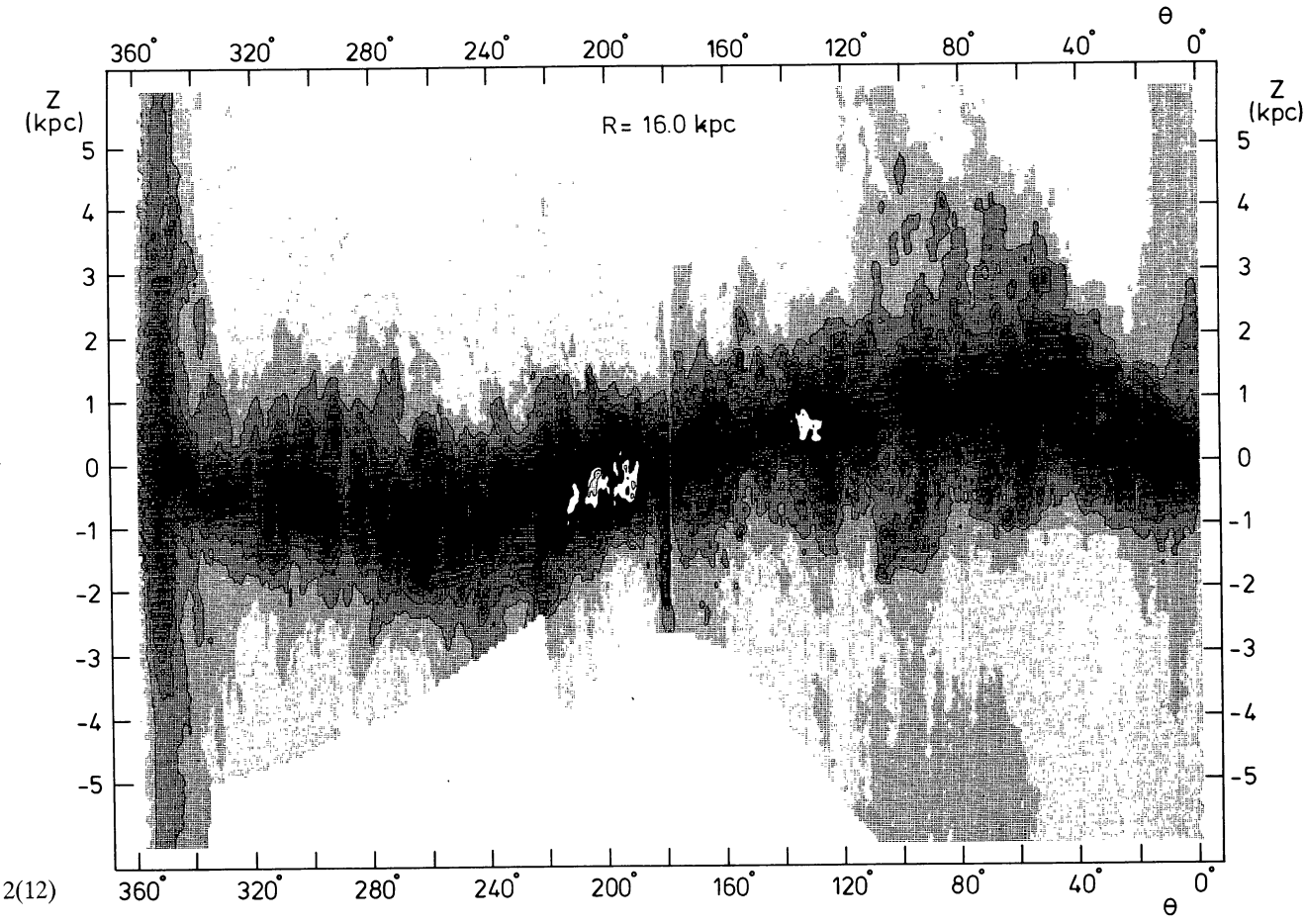

2(12)

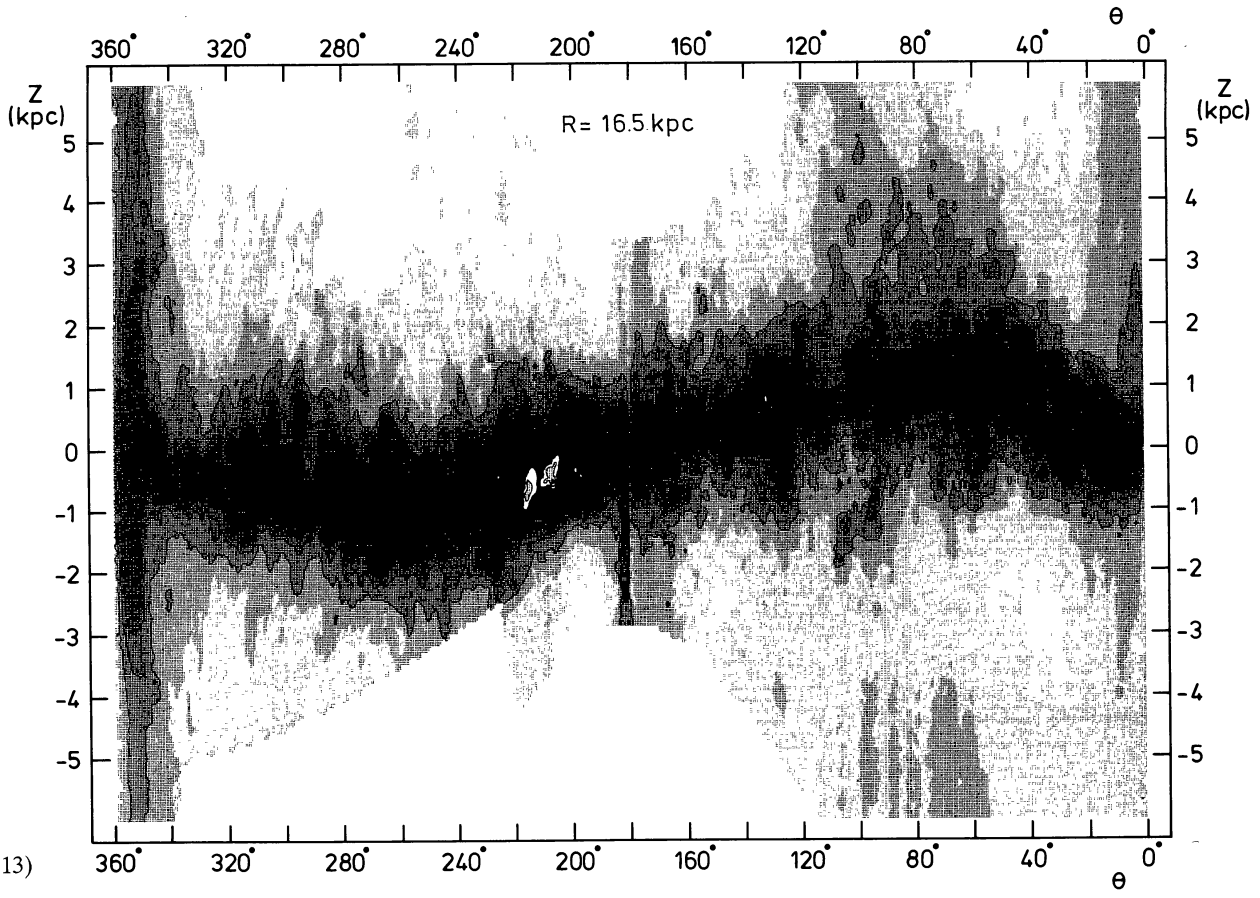

2(13)

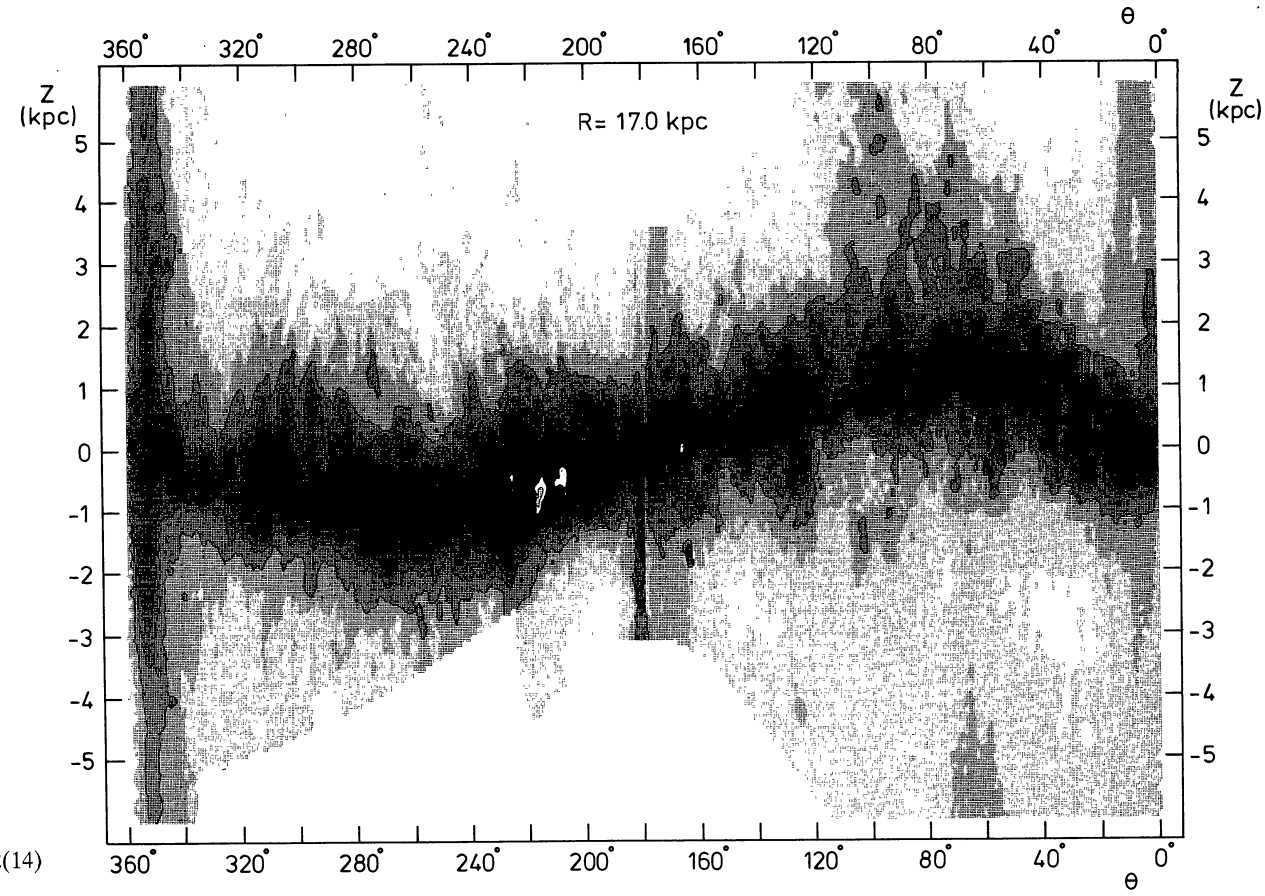

2(14)

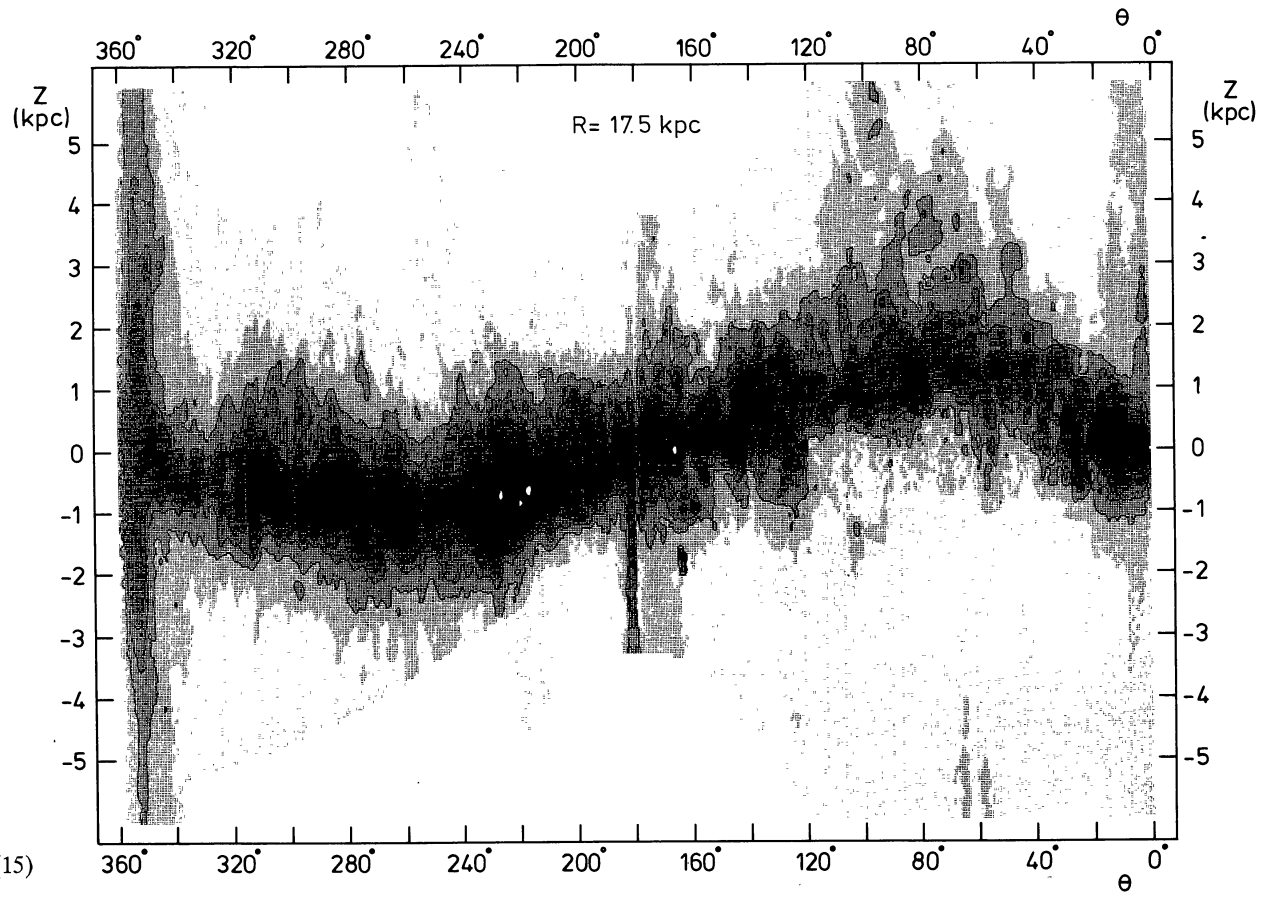

2(15)

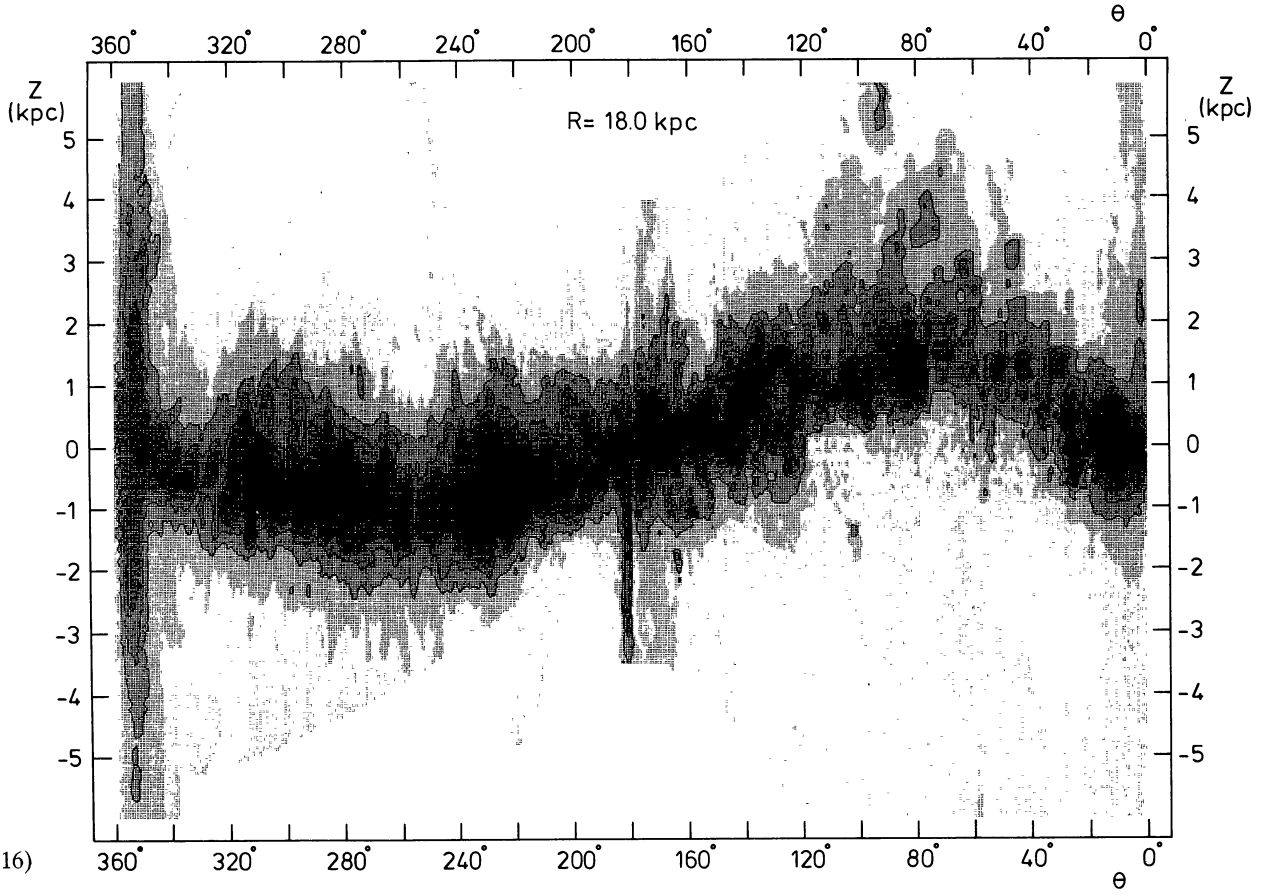

2(16)

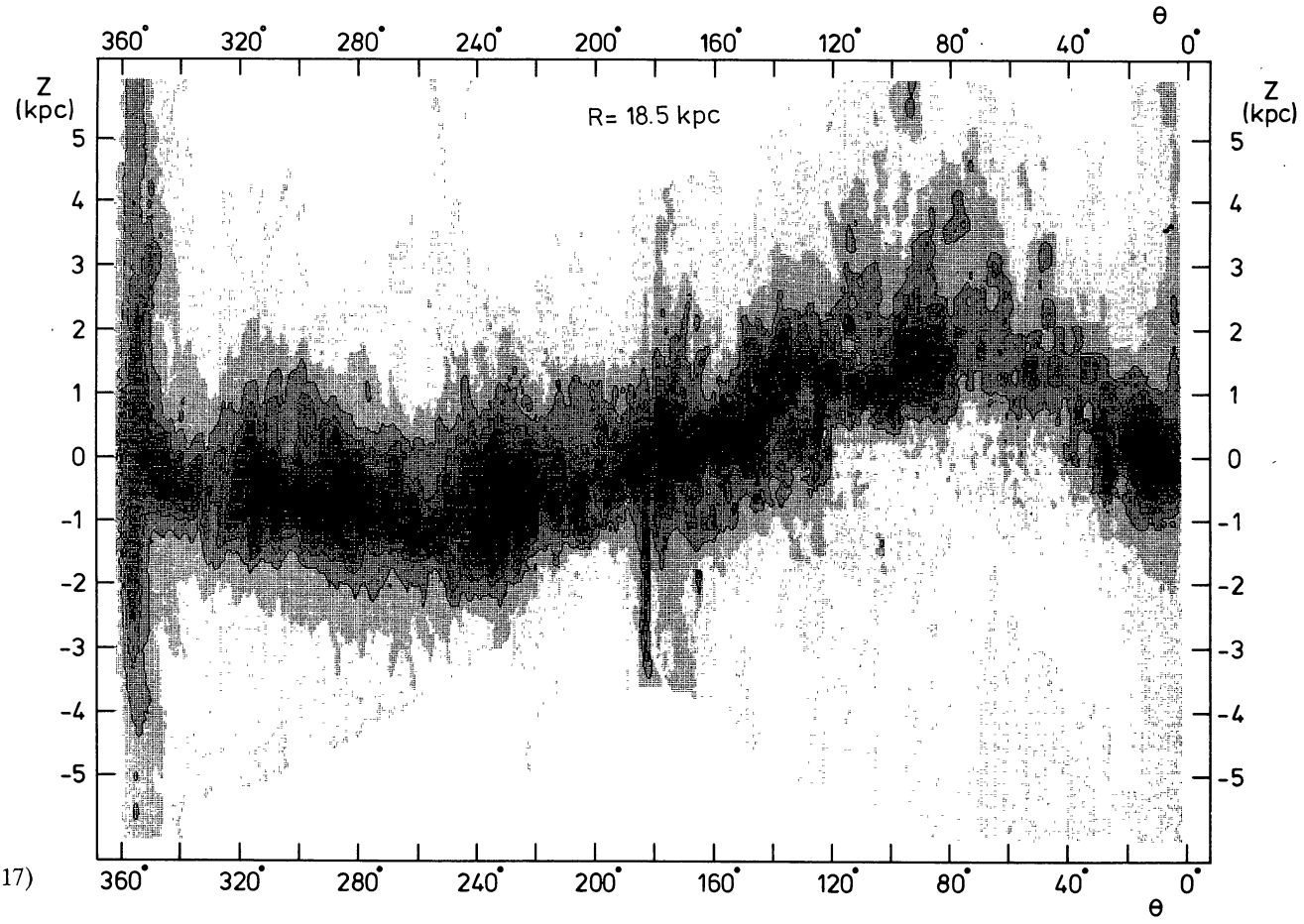

2(17)

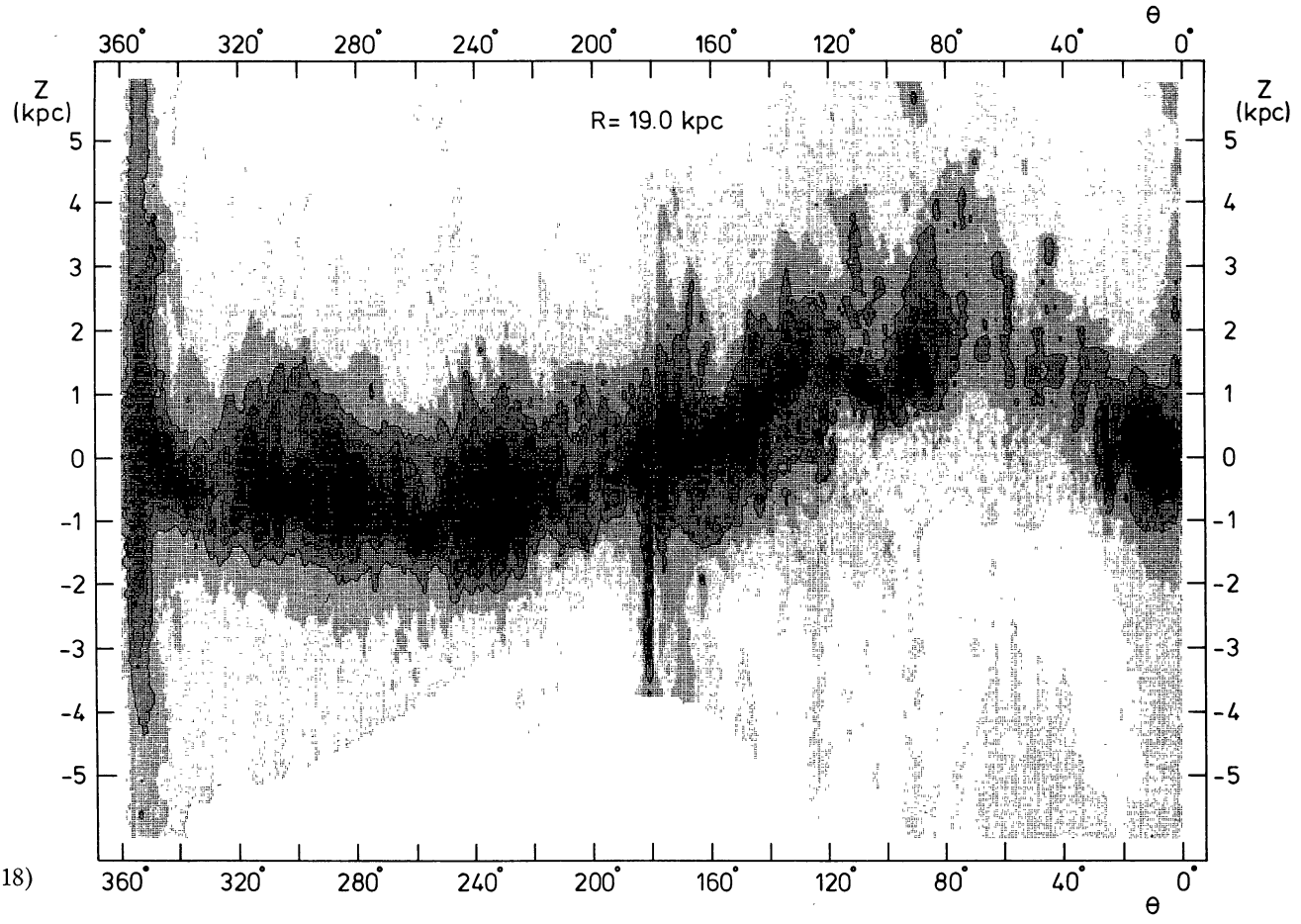

2(18)

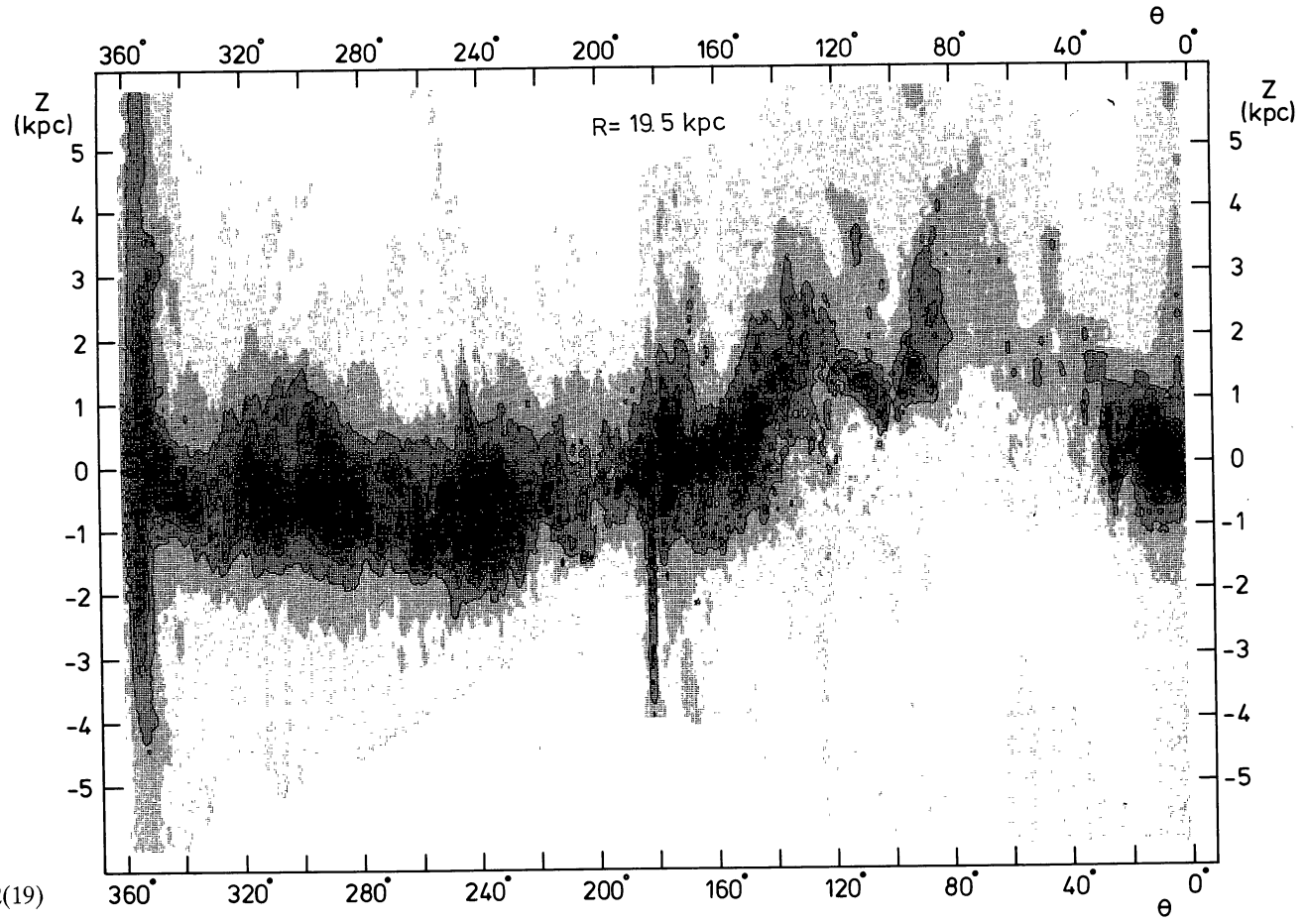

2(19)

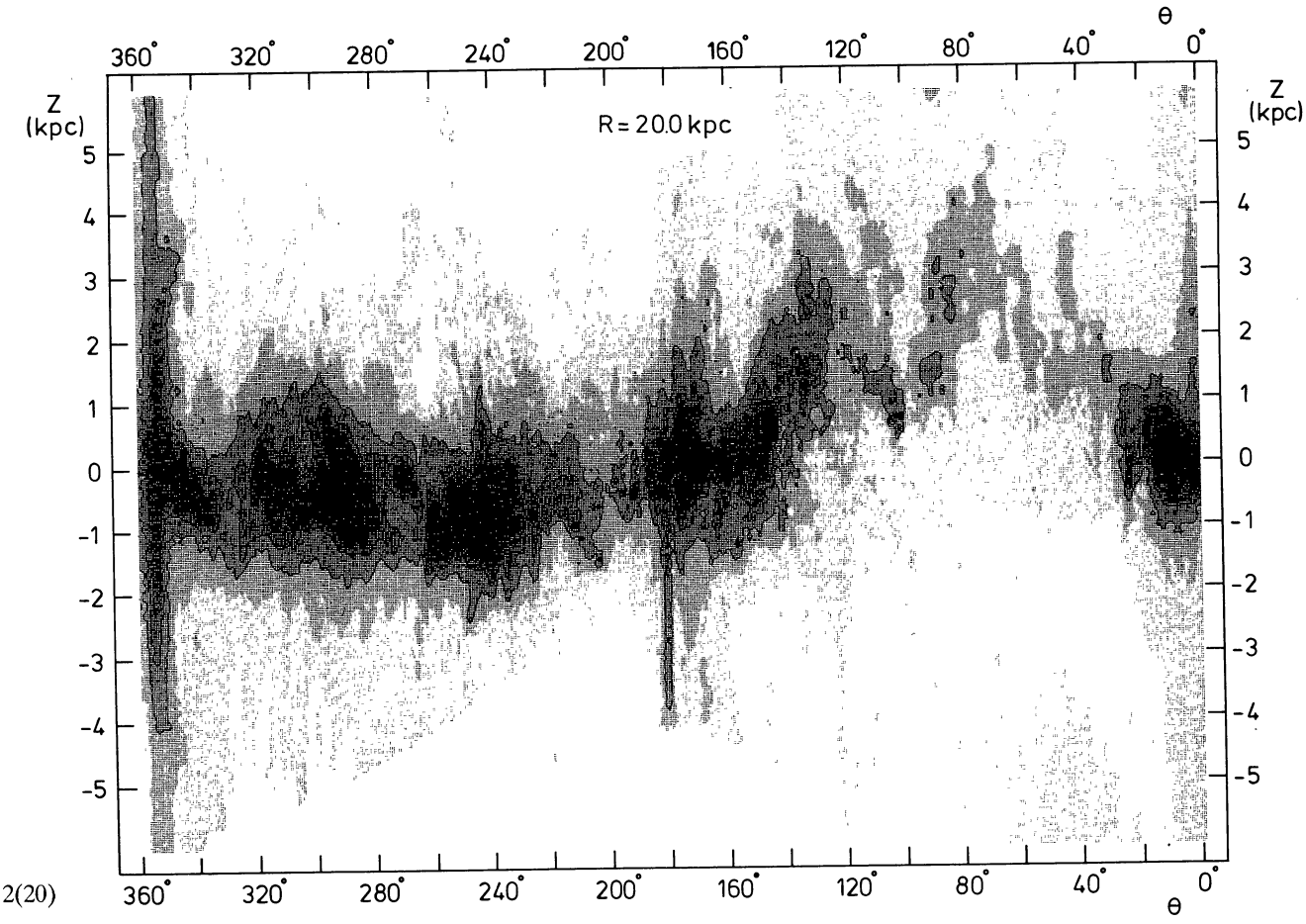

2(20)

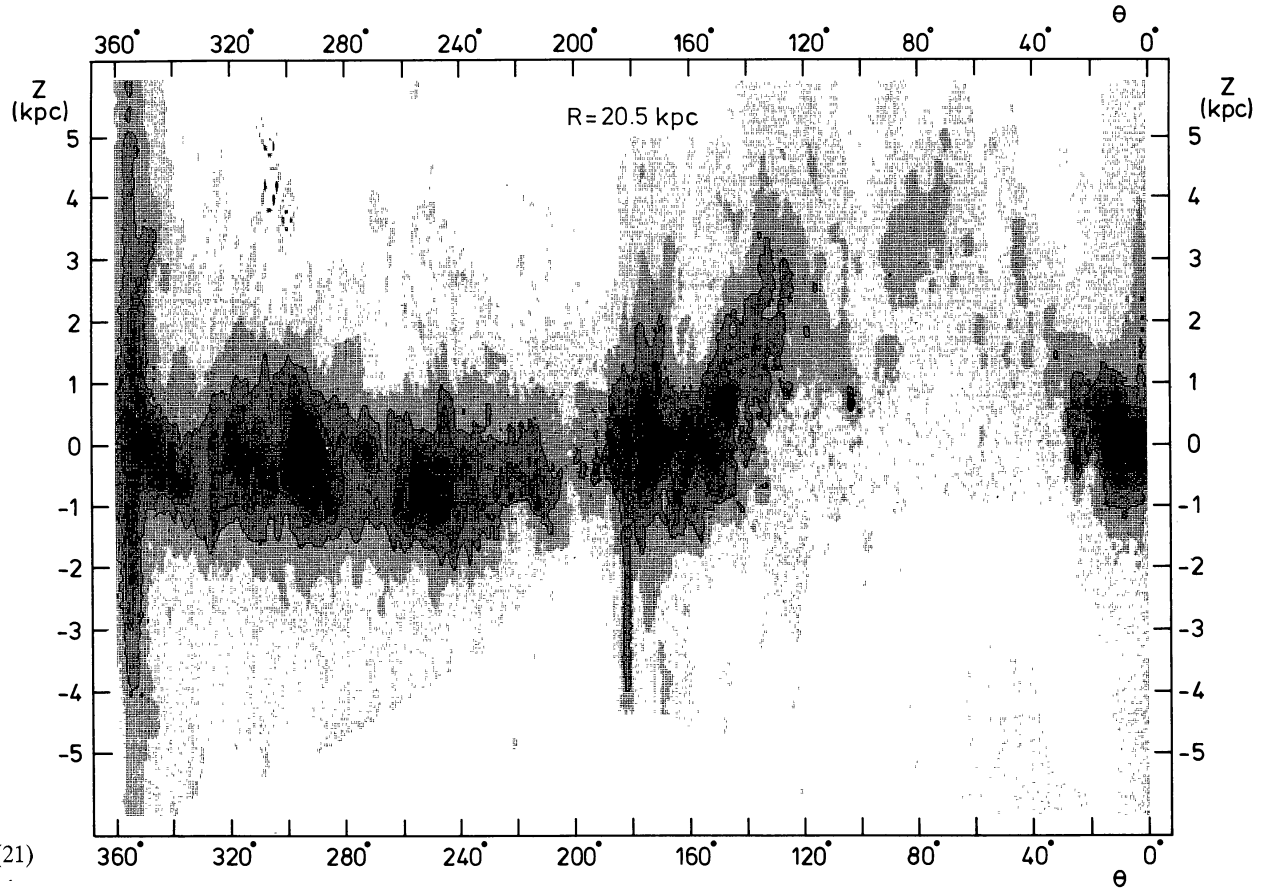

2(21)

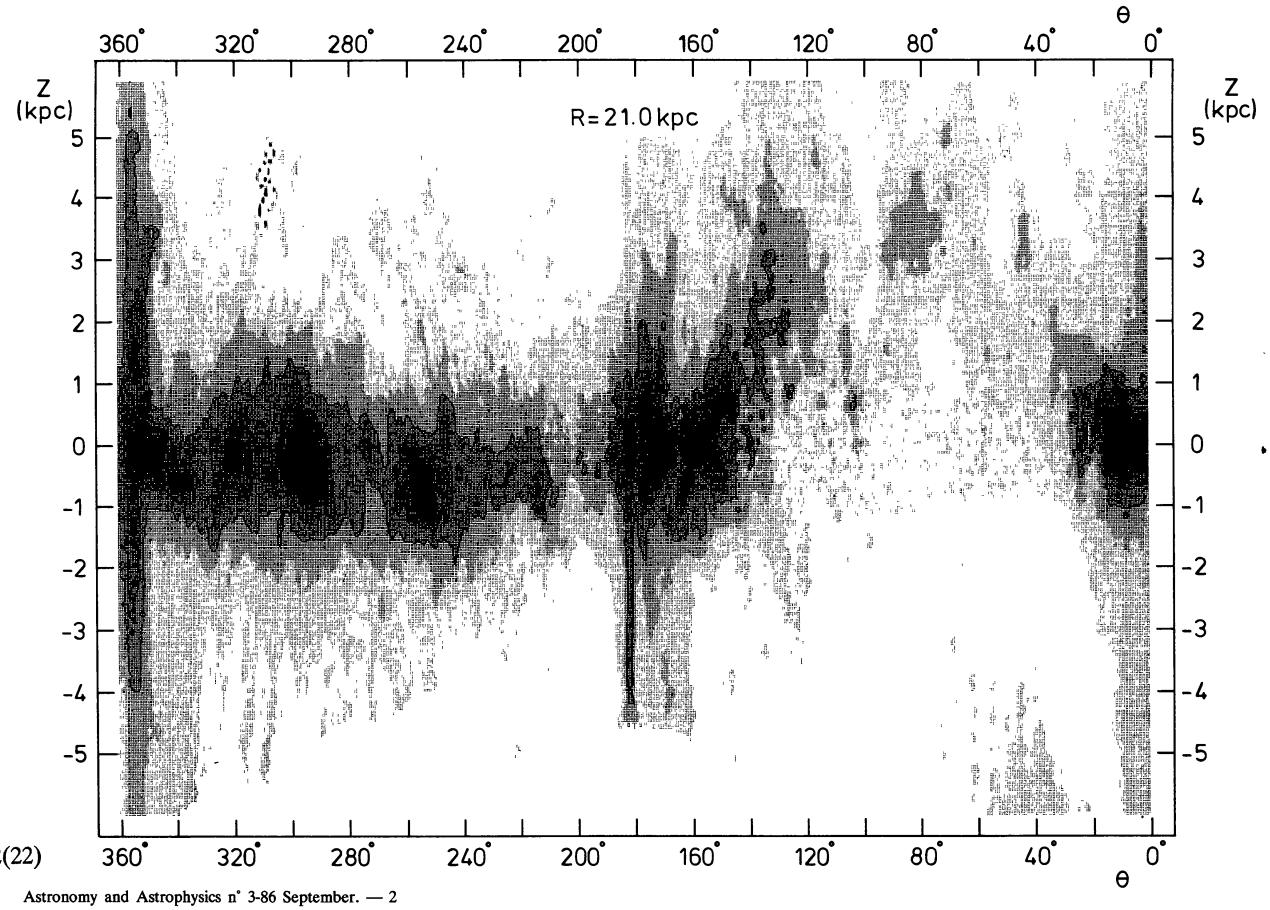

2(22)

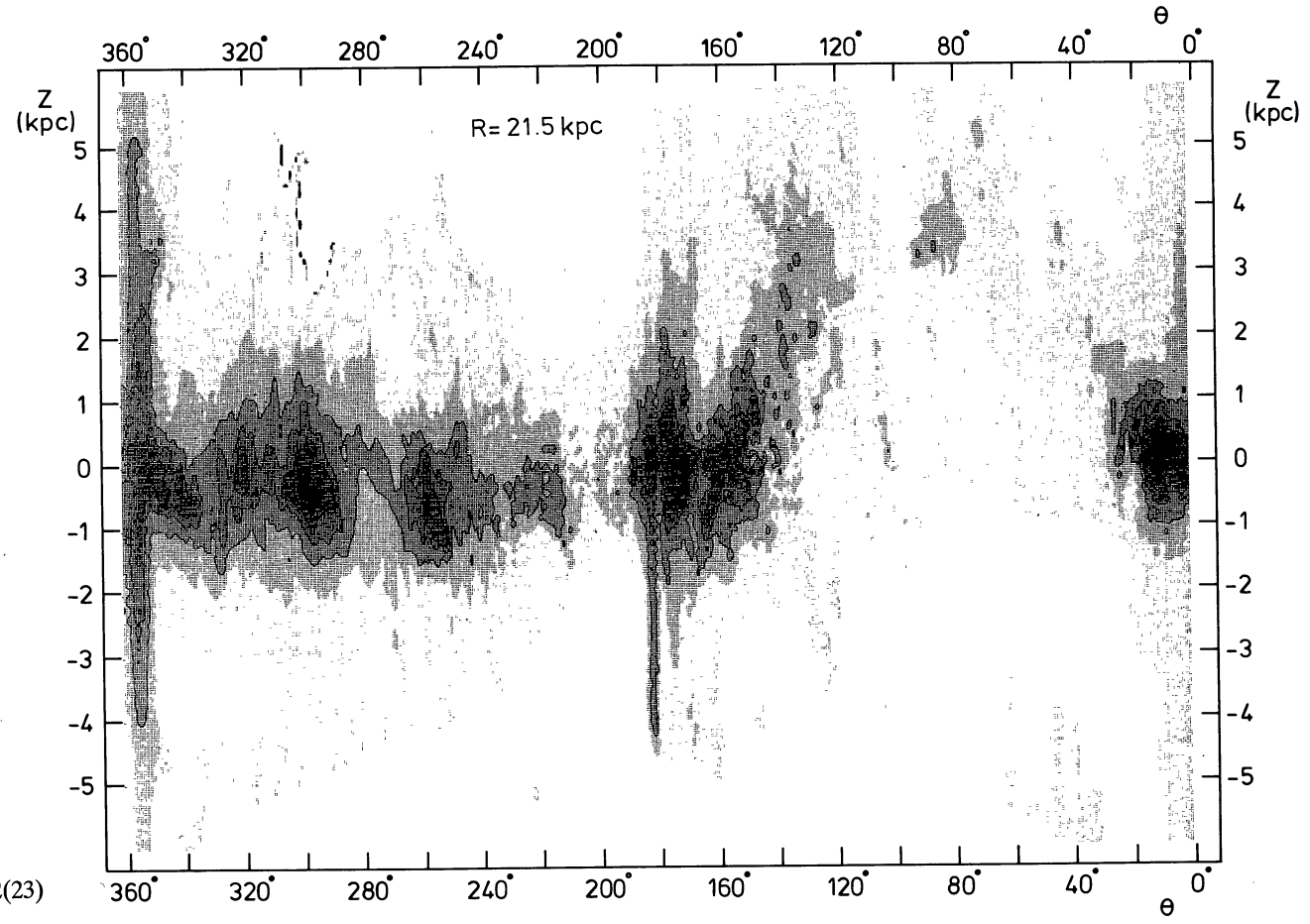

2(23)

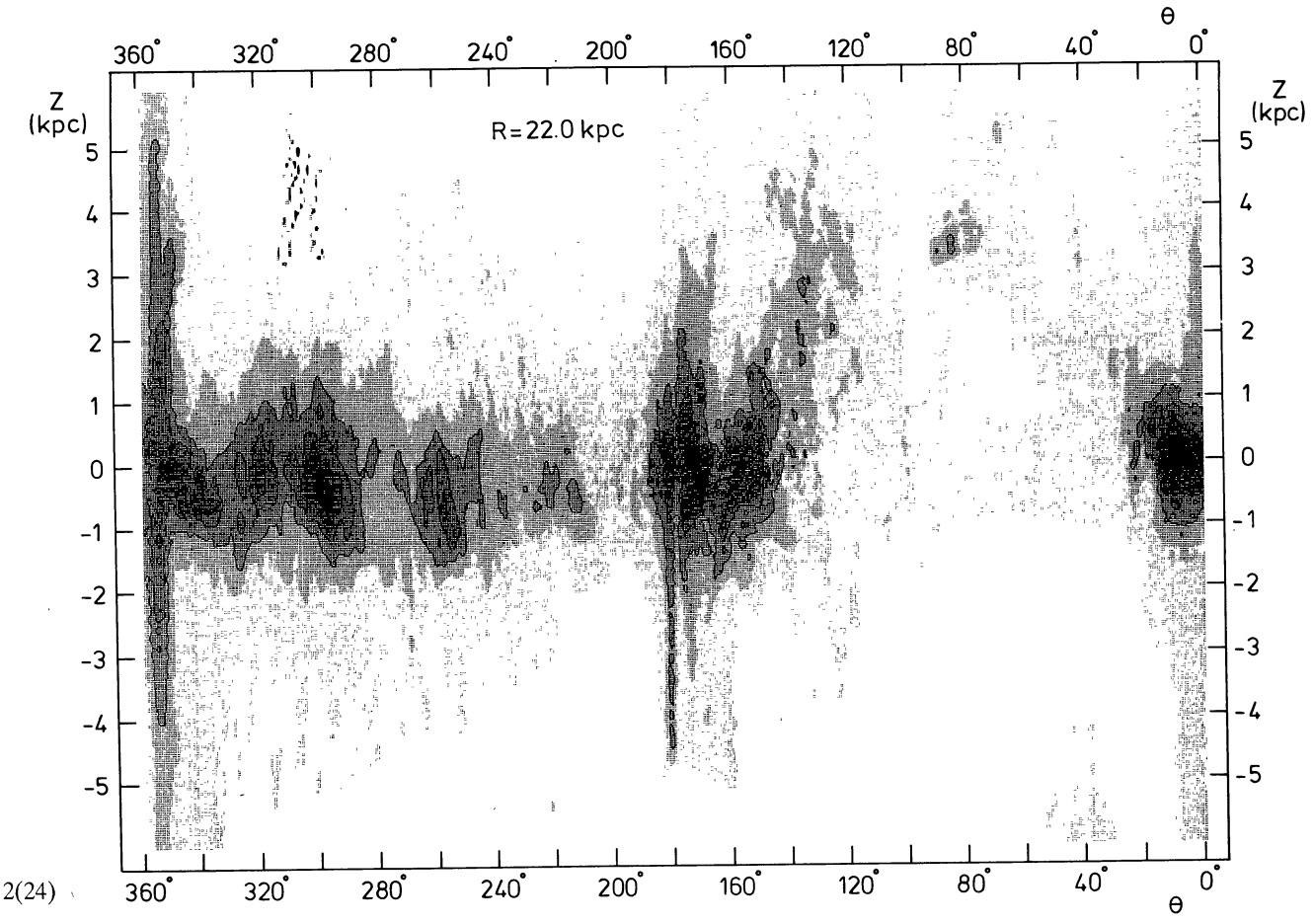

2(24)

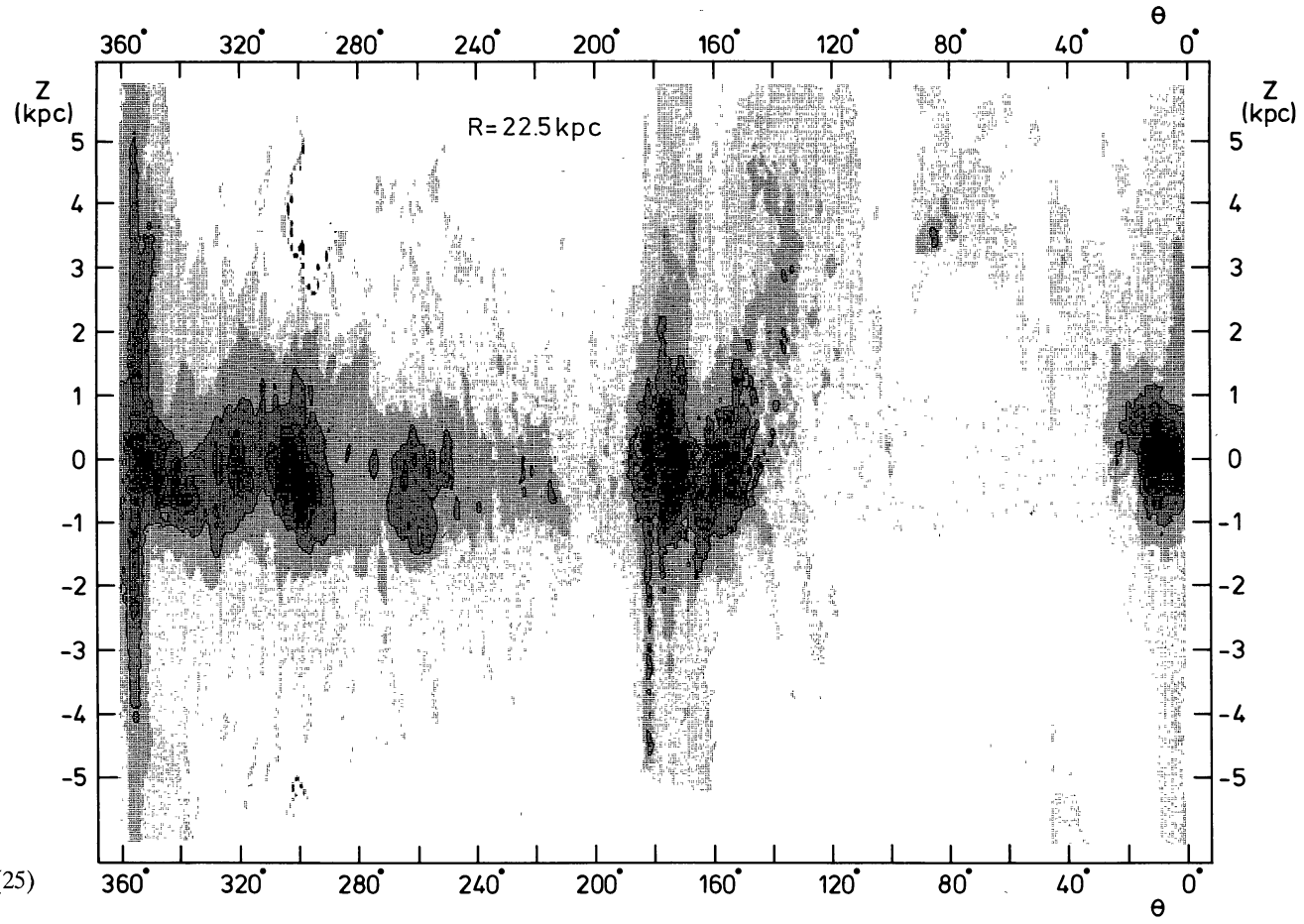

2(25)

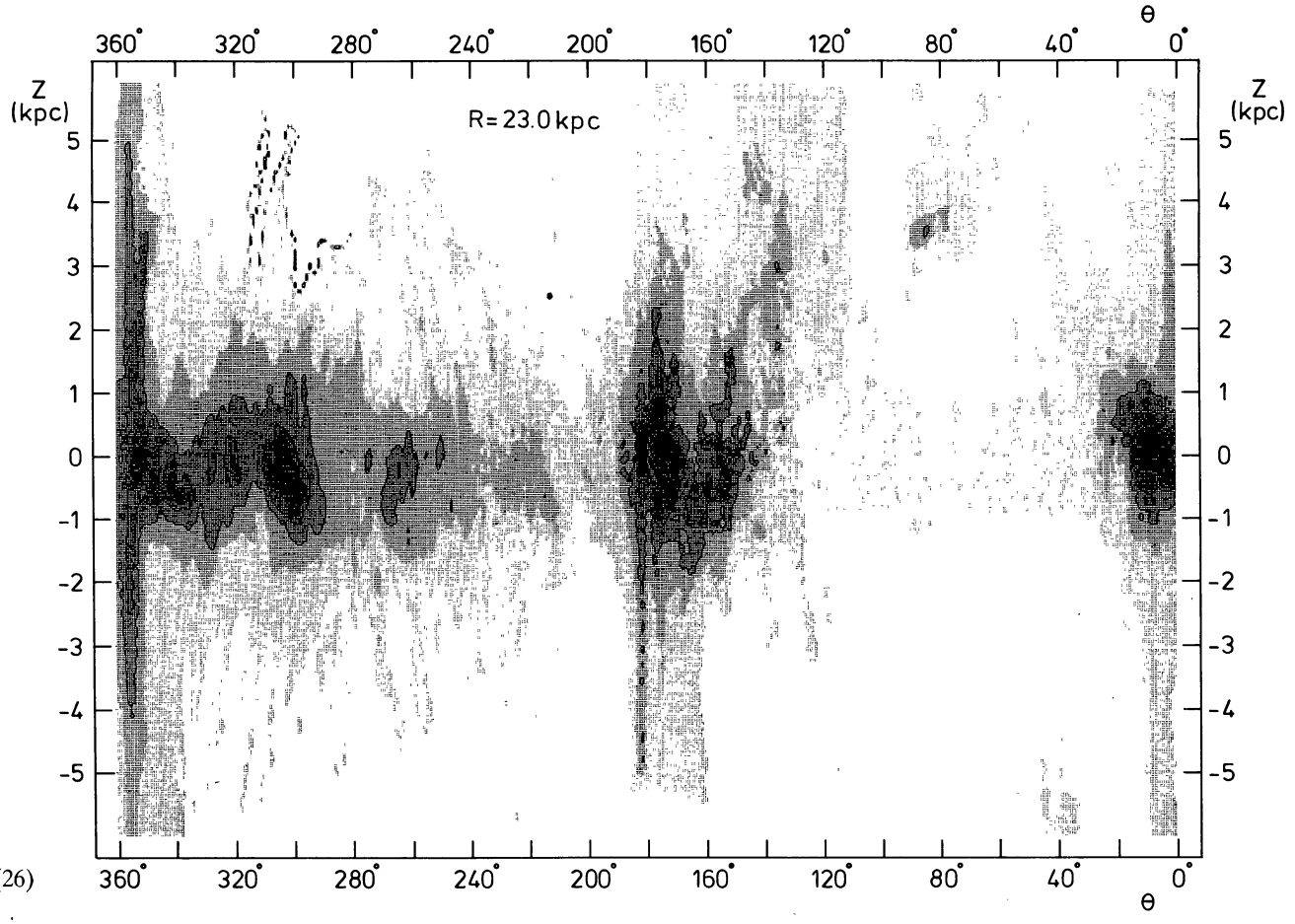

2(26)

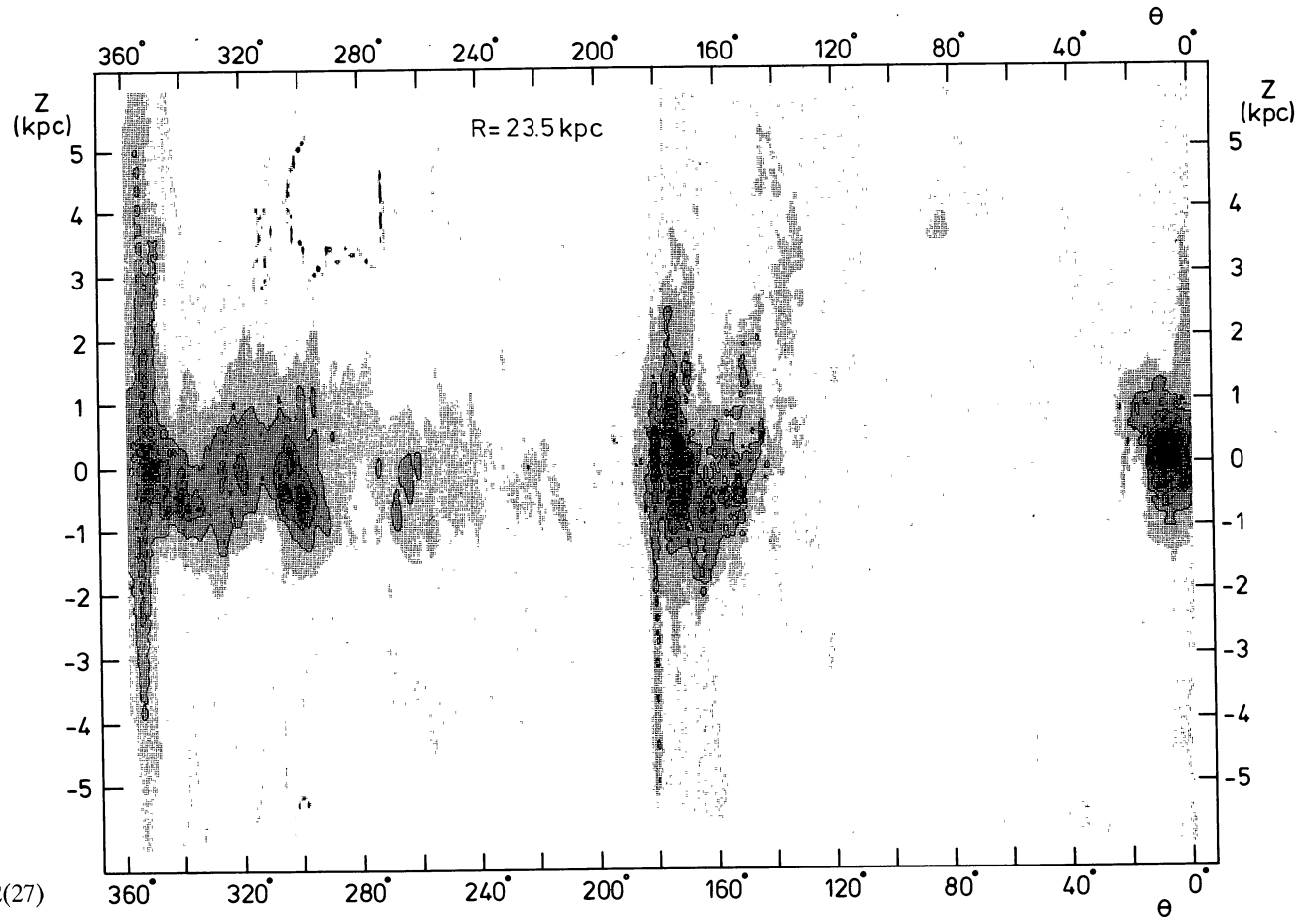

2(27)

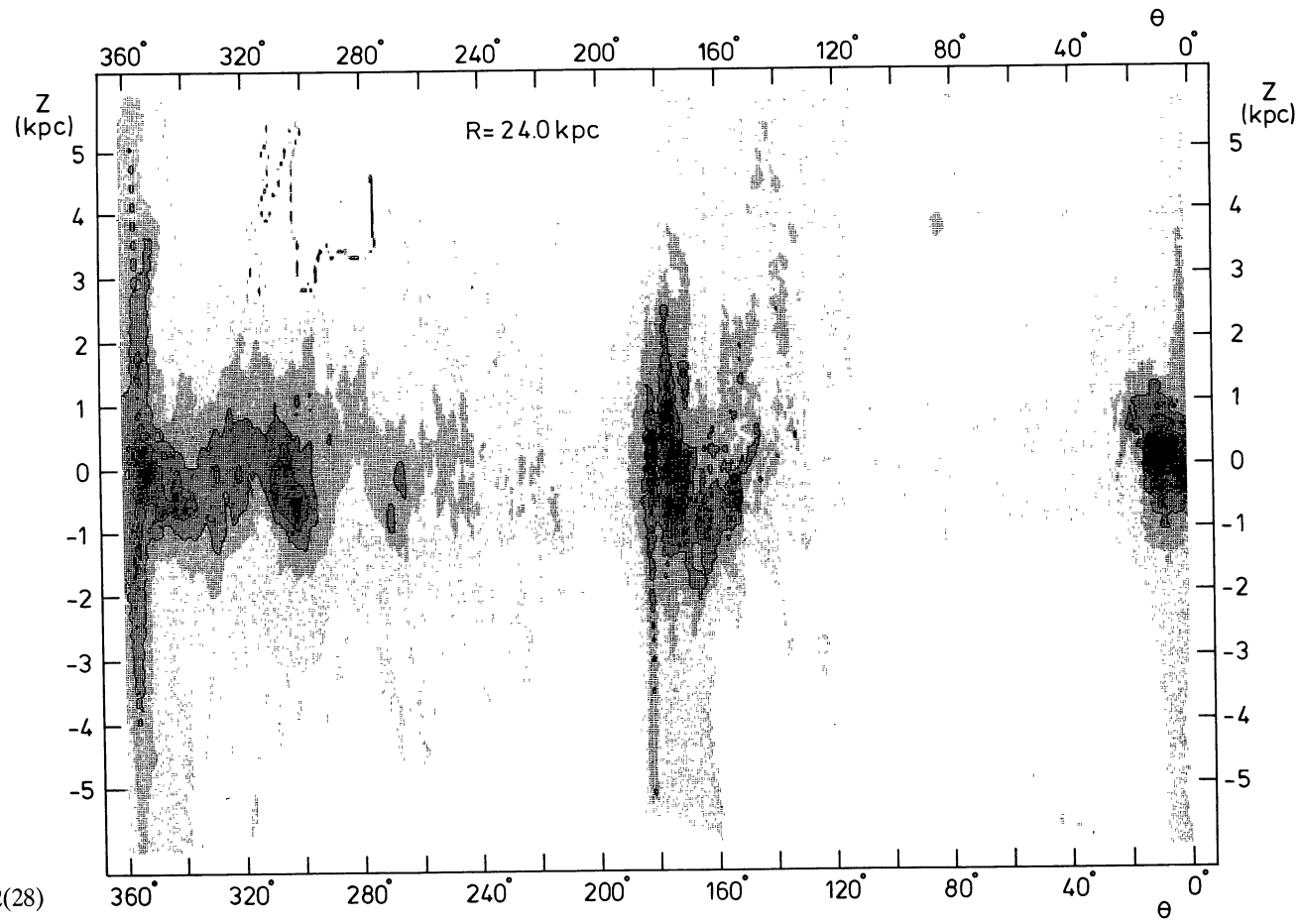

2(28)

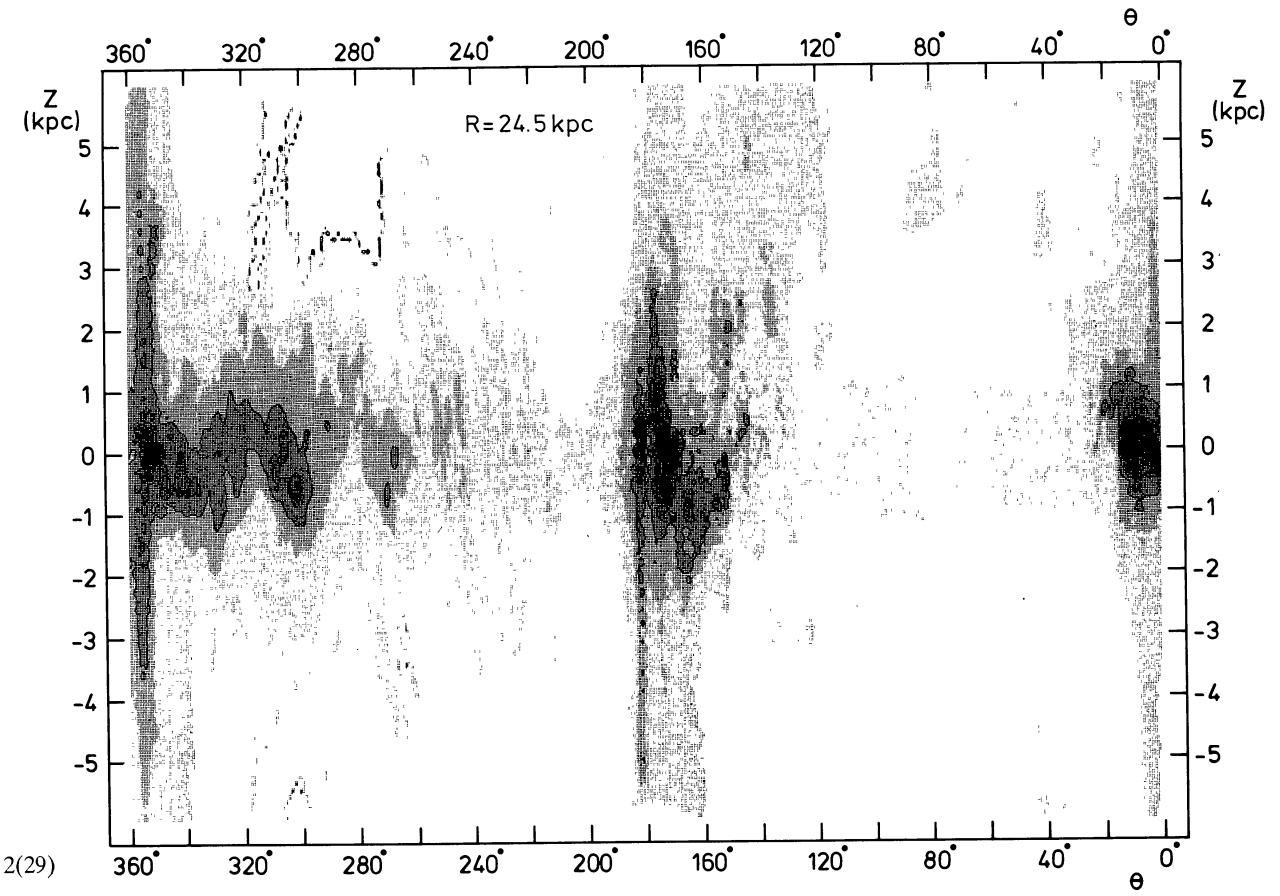

2(29)

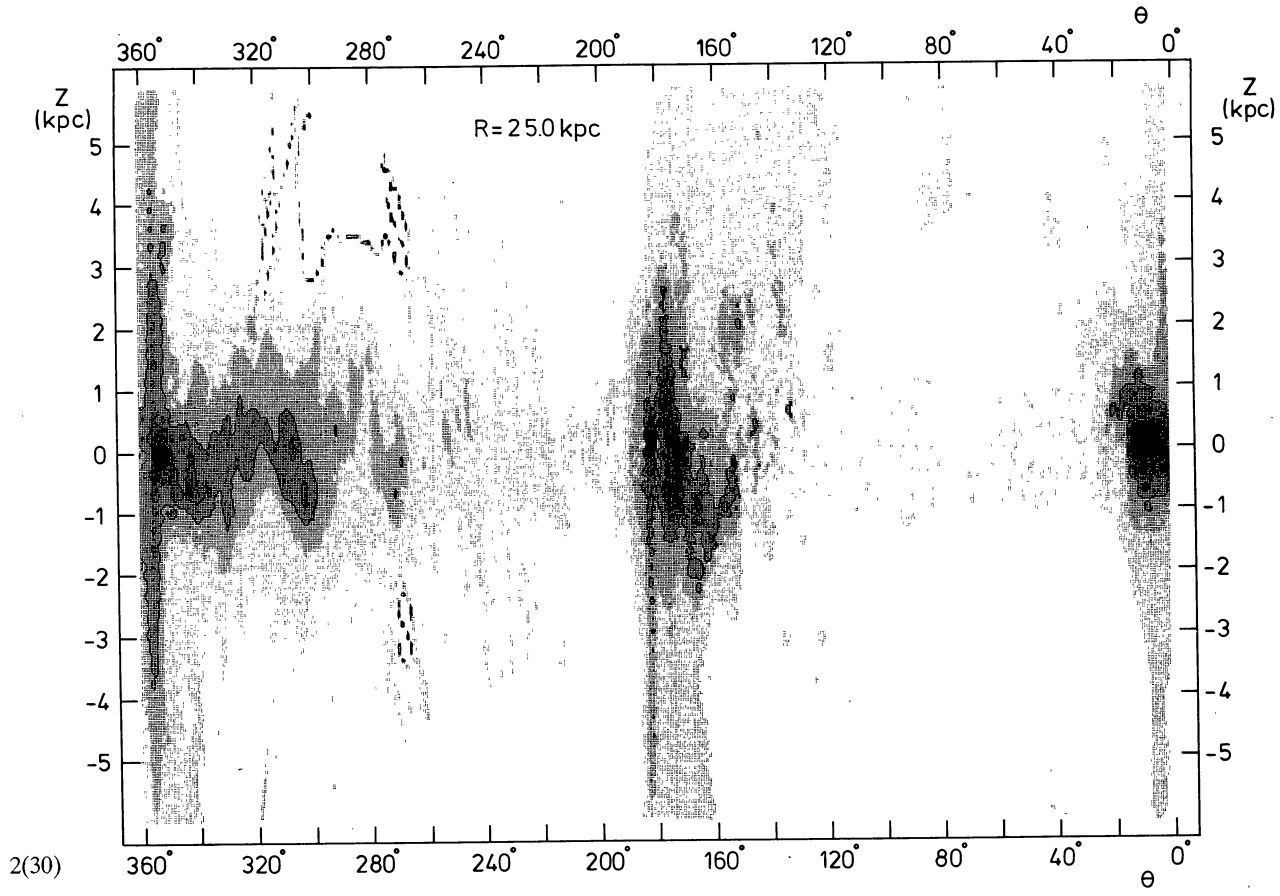

2(30)

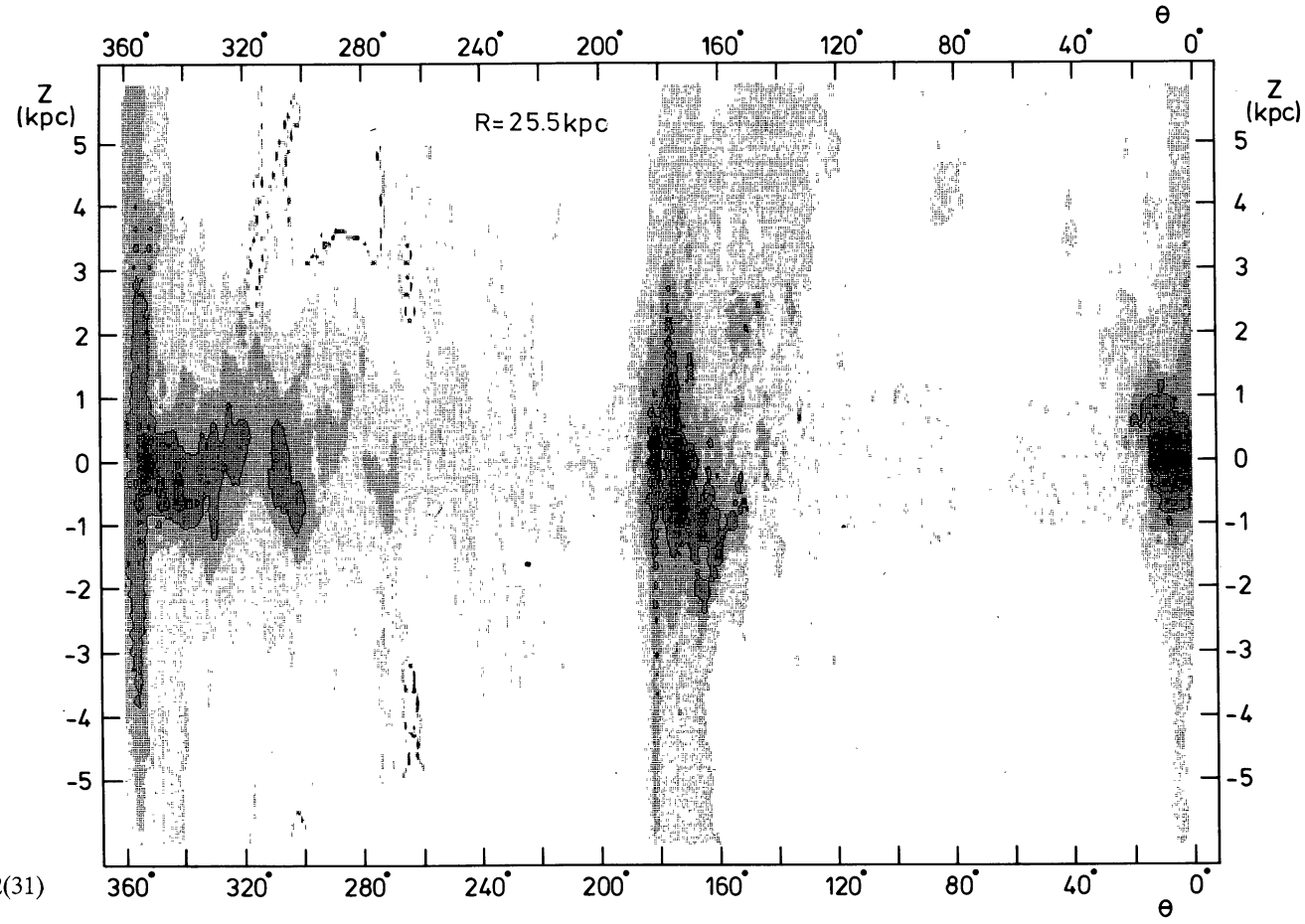

2(31)

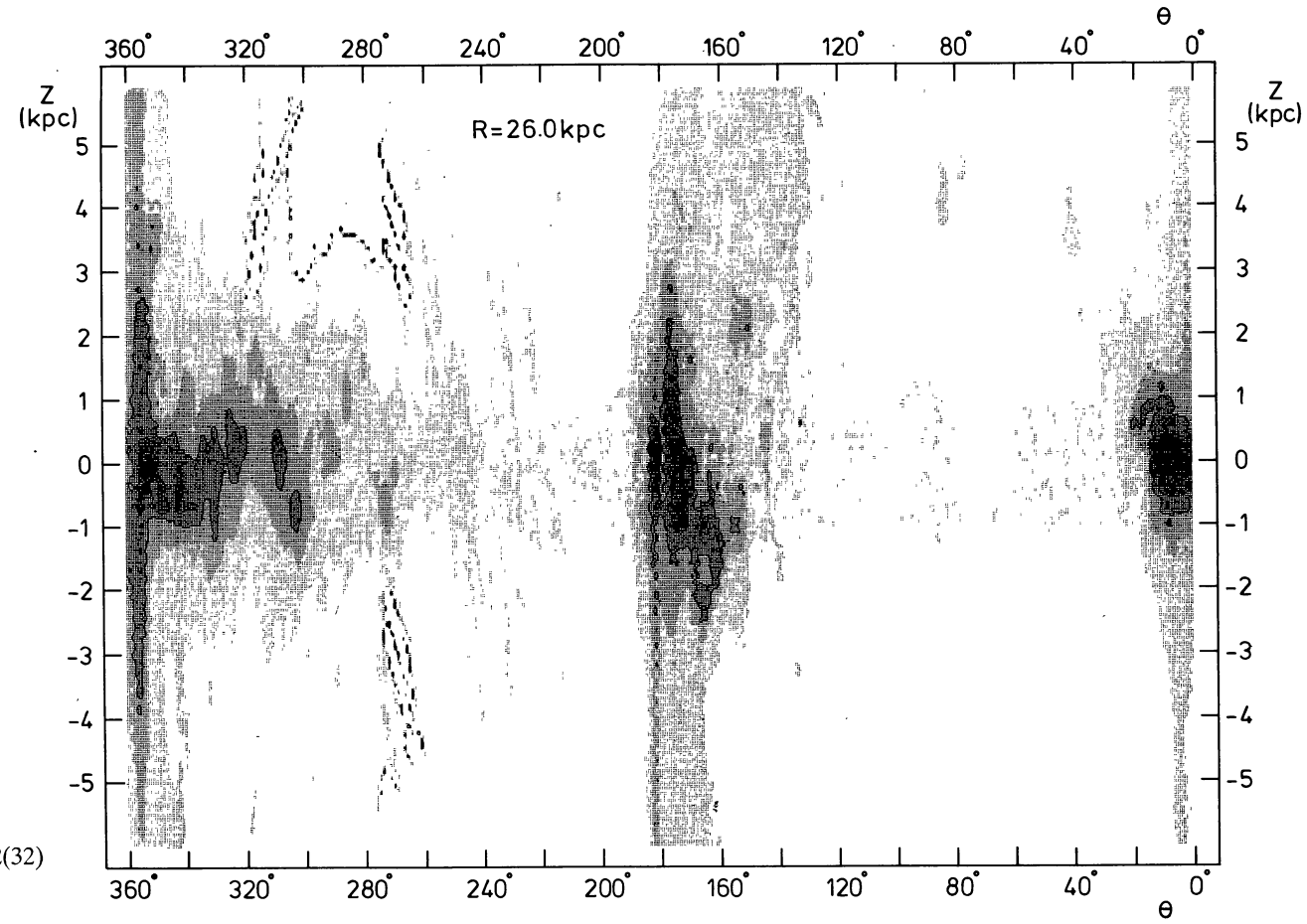

2(32)

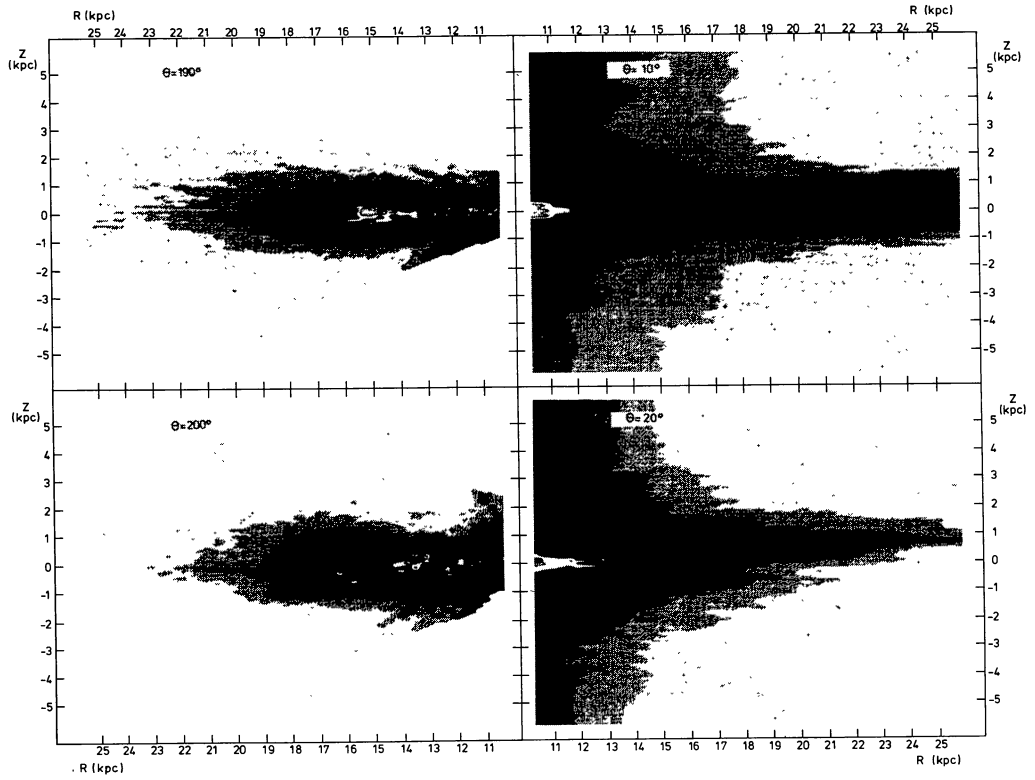

3(1)

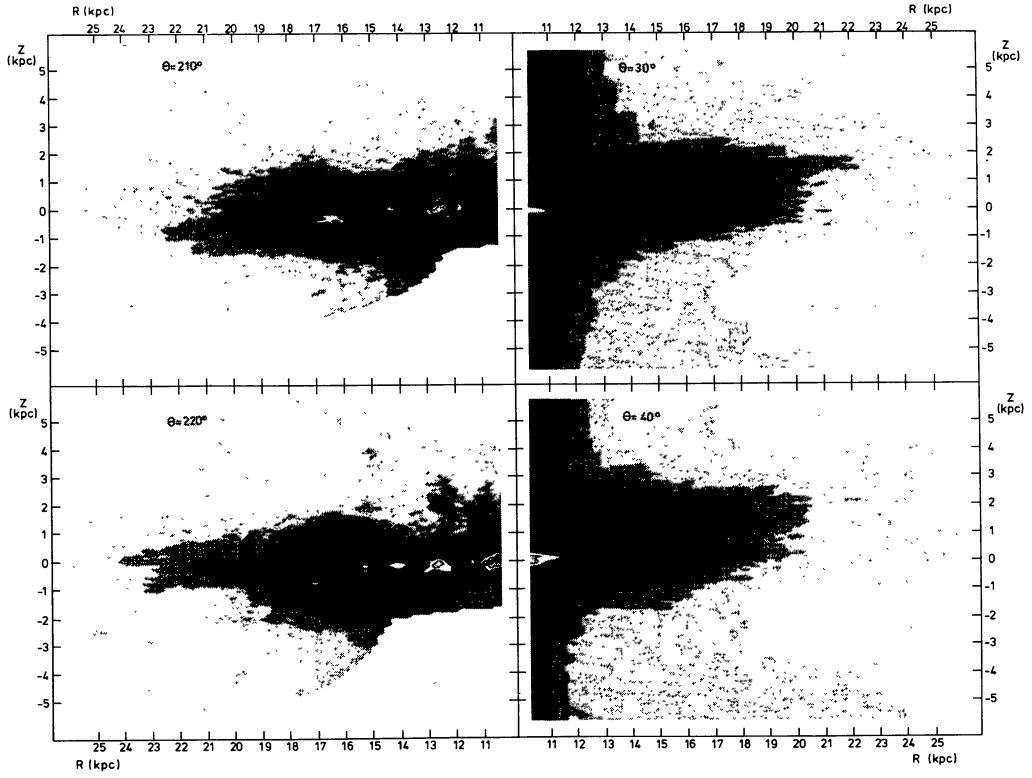

3(2)

FIGURES 3(1)-3(14). — $R, z \mid_\theta$ maps showing arrangement of hydrogen volume densities in sheets through the galactic center perpendicular to its equator at the indicated galactocentric azimuths θ. Contours and grey-scale levels are drawn at the same values as in figure 1. The cylindrical-coordinate R, θ, z data cube was sampled at 100 pc intervals in z and 250 pc intervals in R ; the range in azimuth is $\pm 0°5$ centred on the indicated value of θ. In each panel of the figure the paired left-side and right-side maps are separated 180° in azimuth in order to represent sheets cutting galactic diameters in the equator. The approximate 2π-symmetry of the galactic warp makes this pairing especially appropriate.

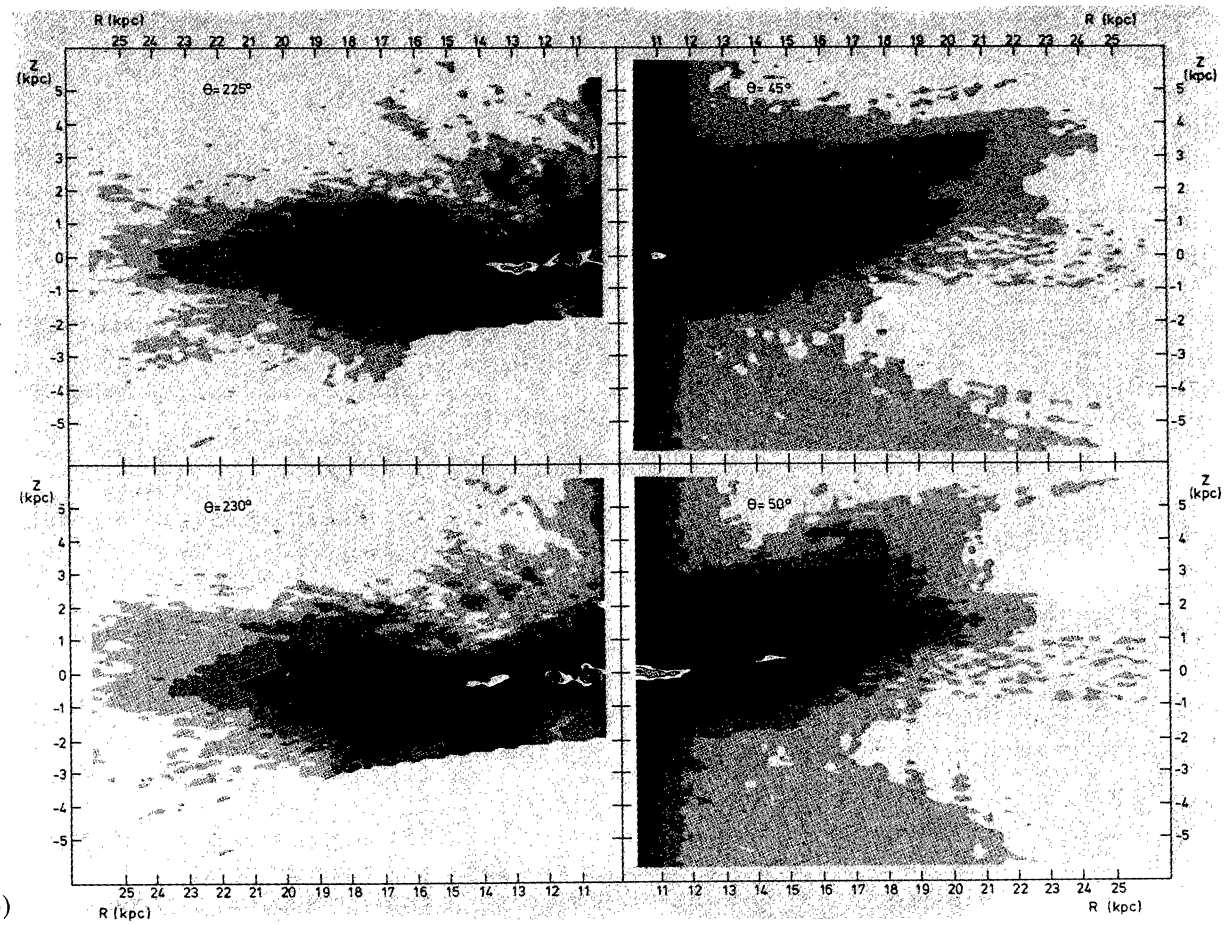

3(3)

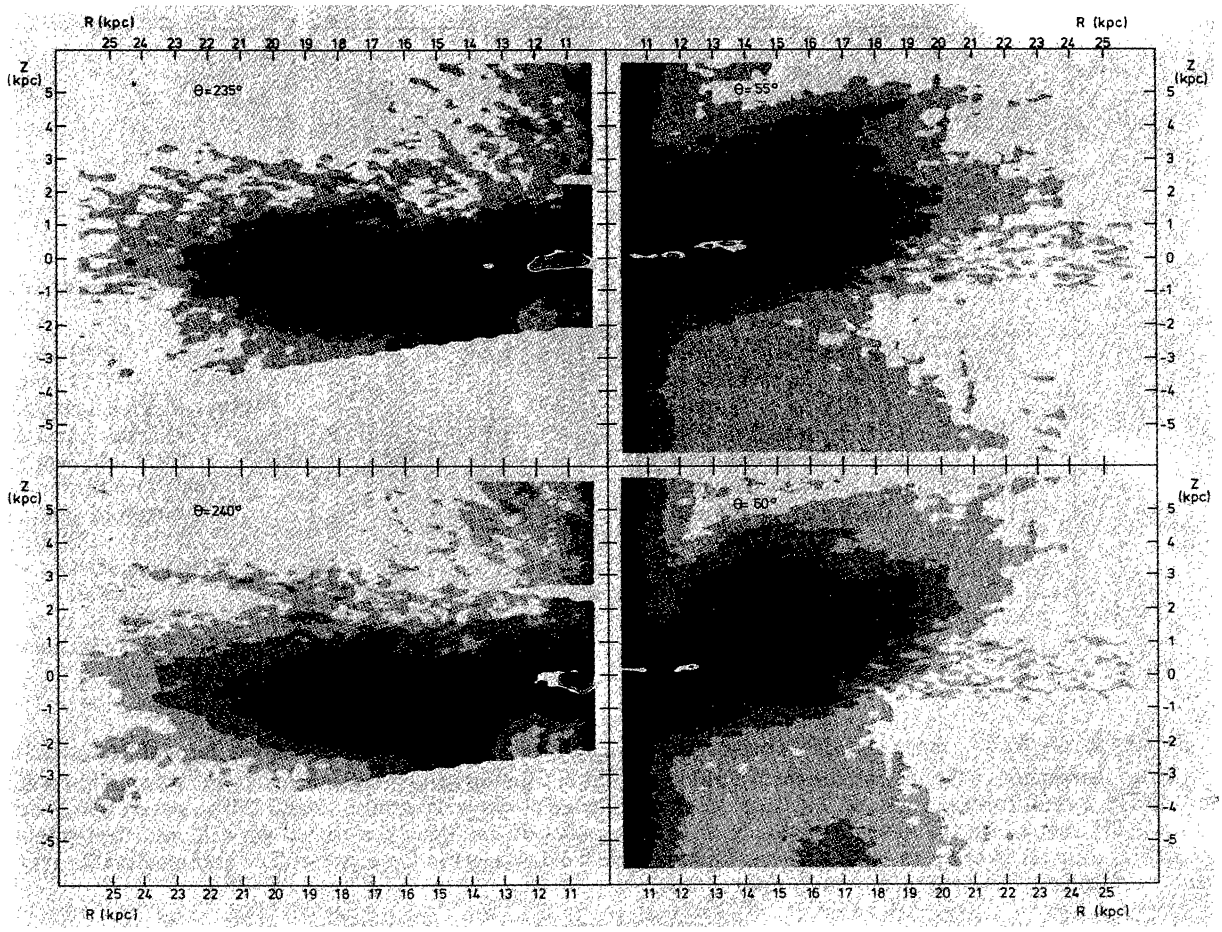

3(4)

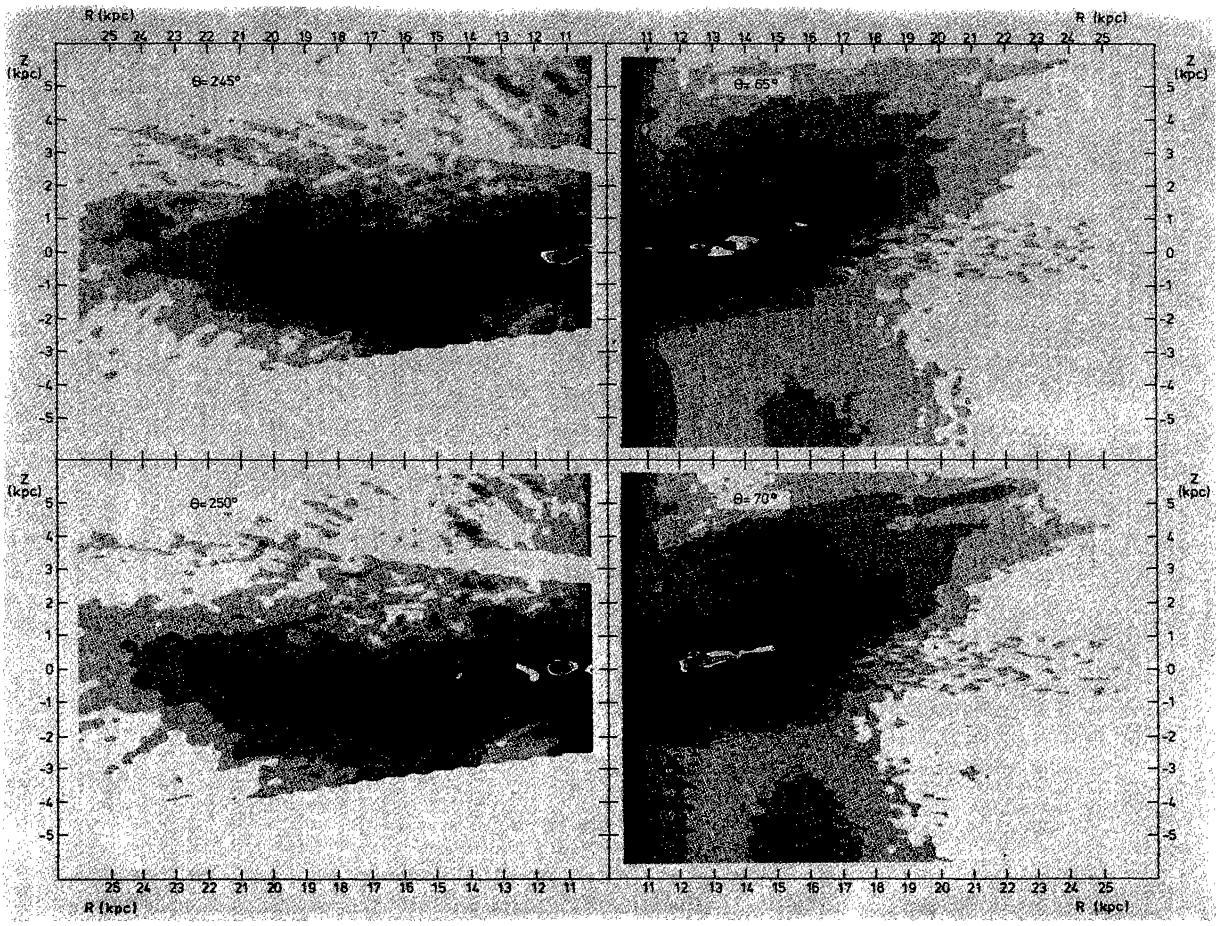

3(5)

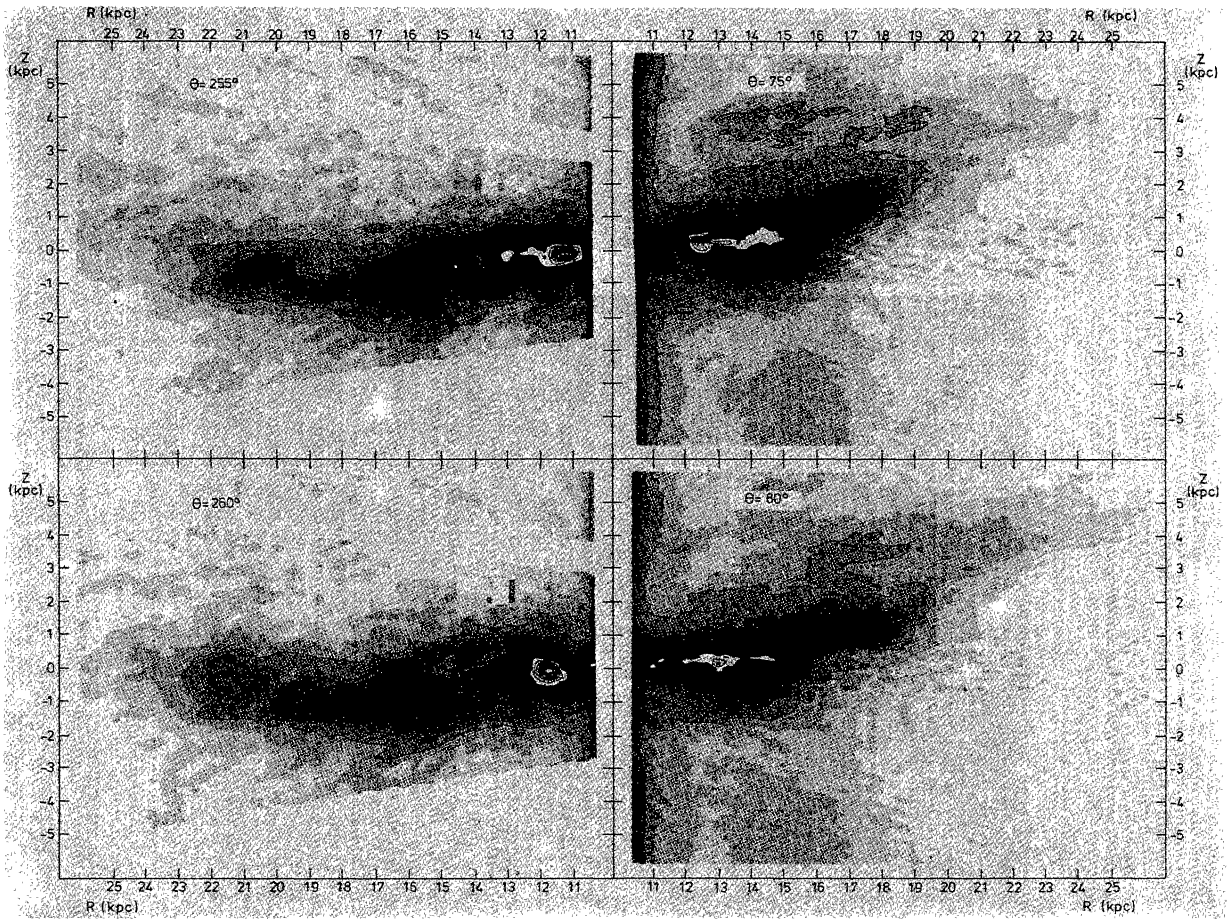

3(6)

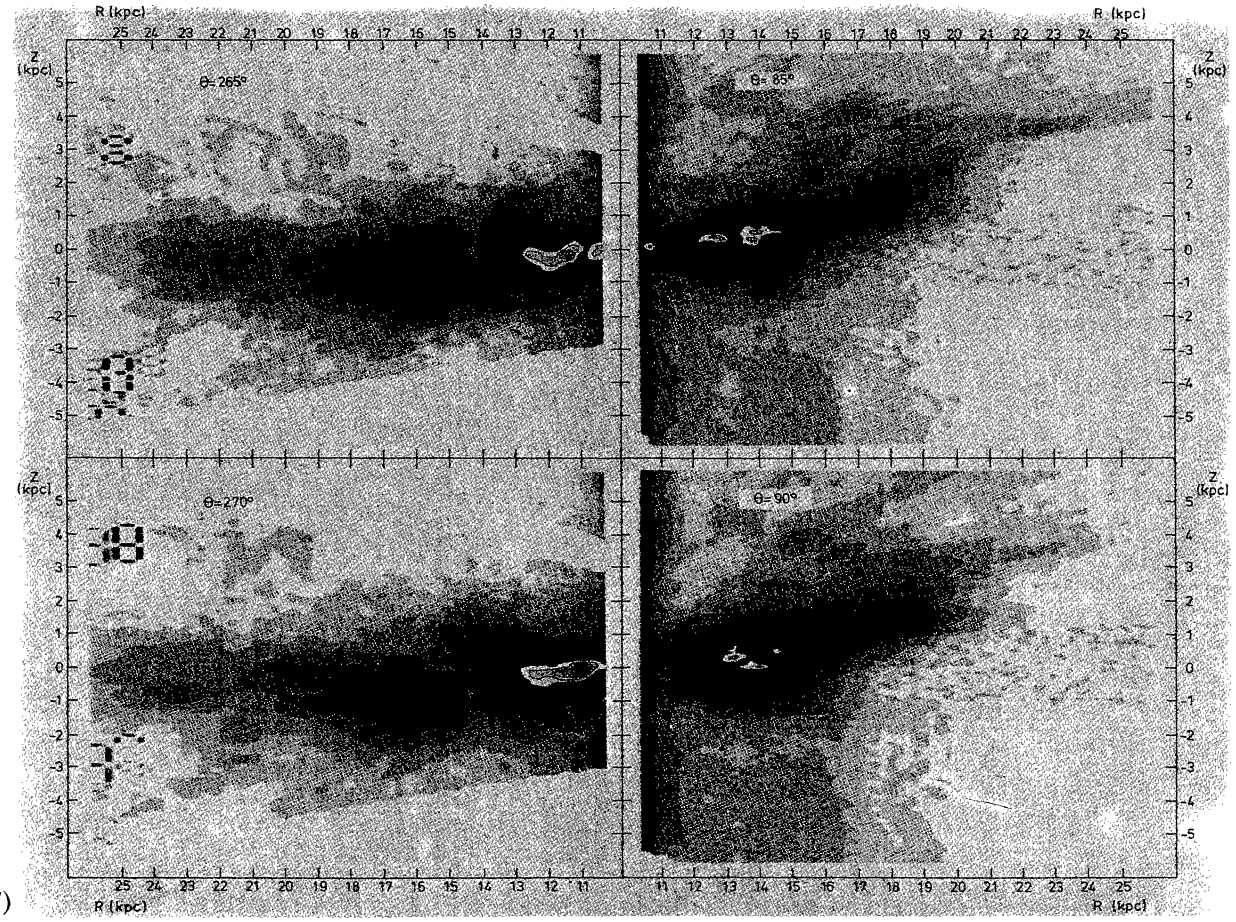

3(7)

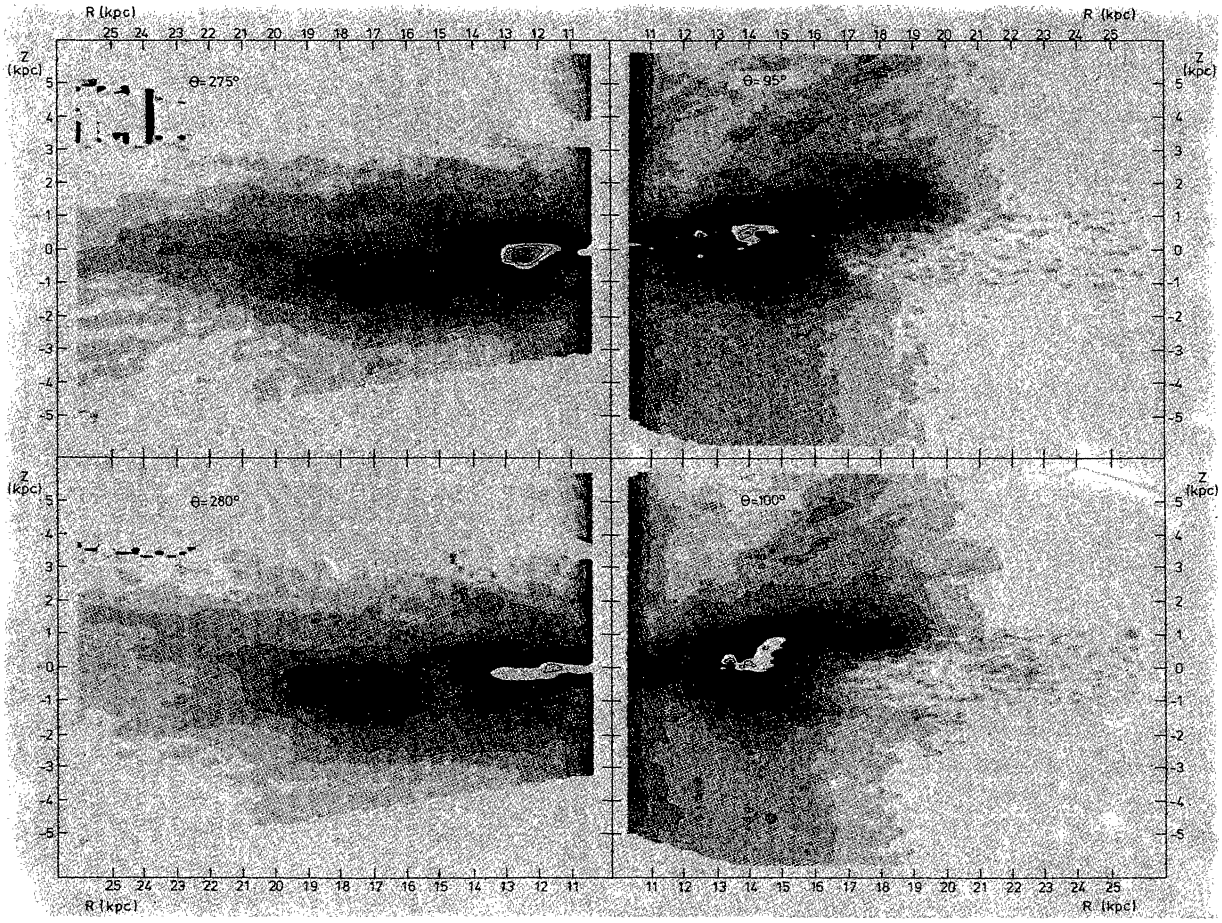

3(8)

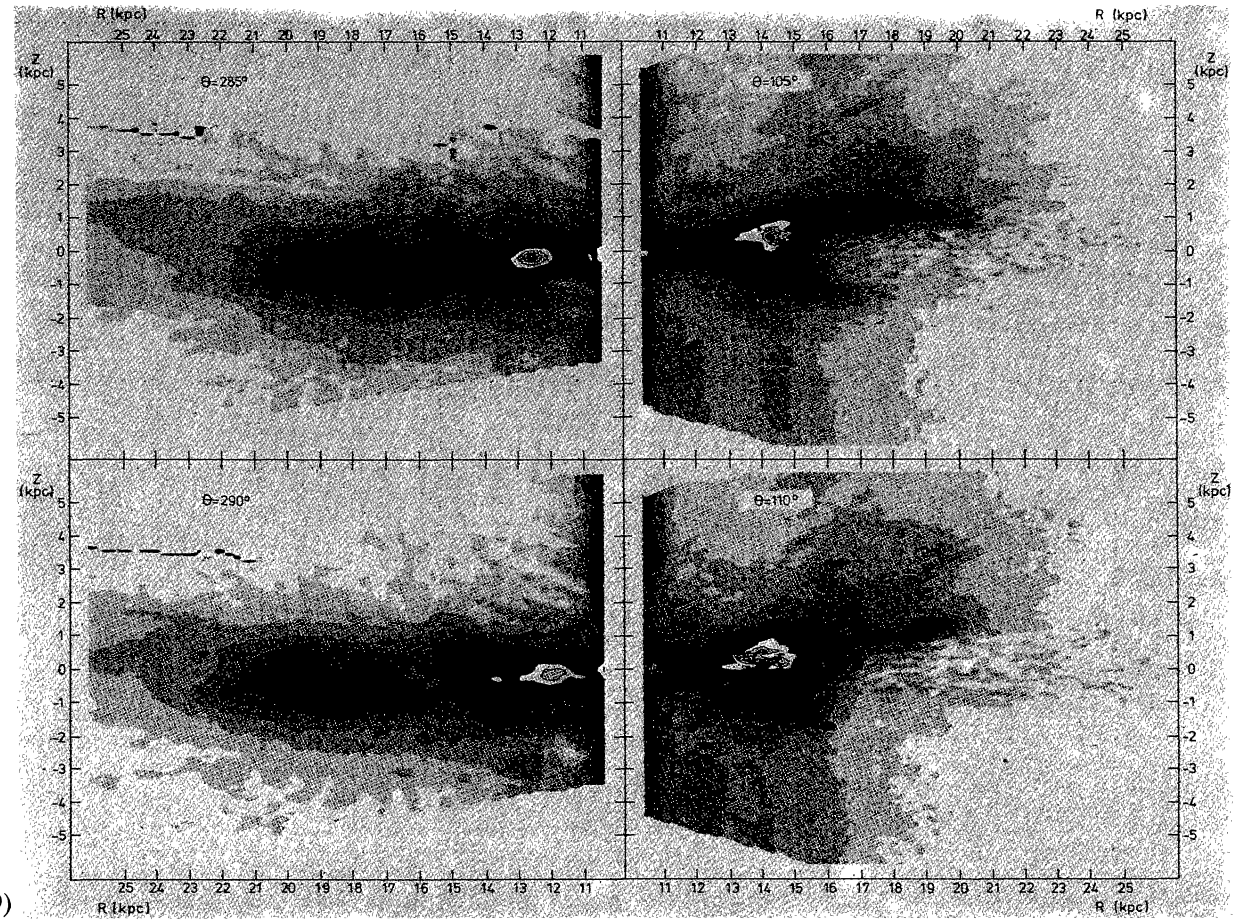

3(9)

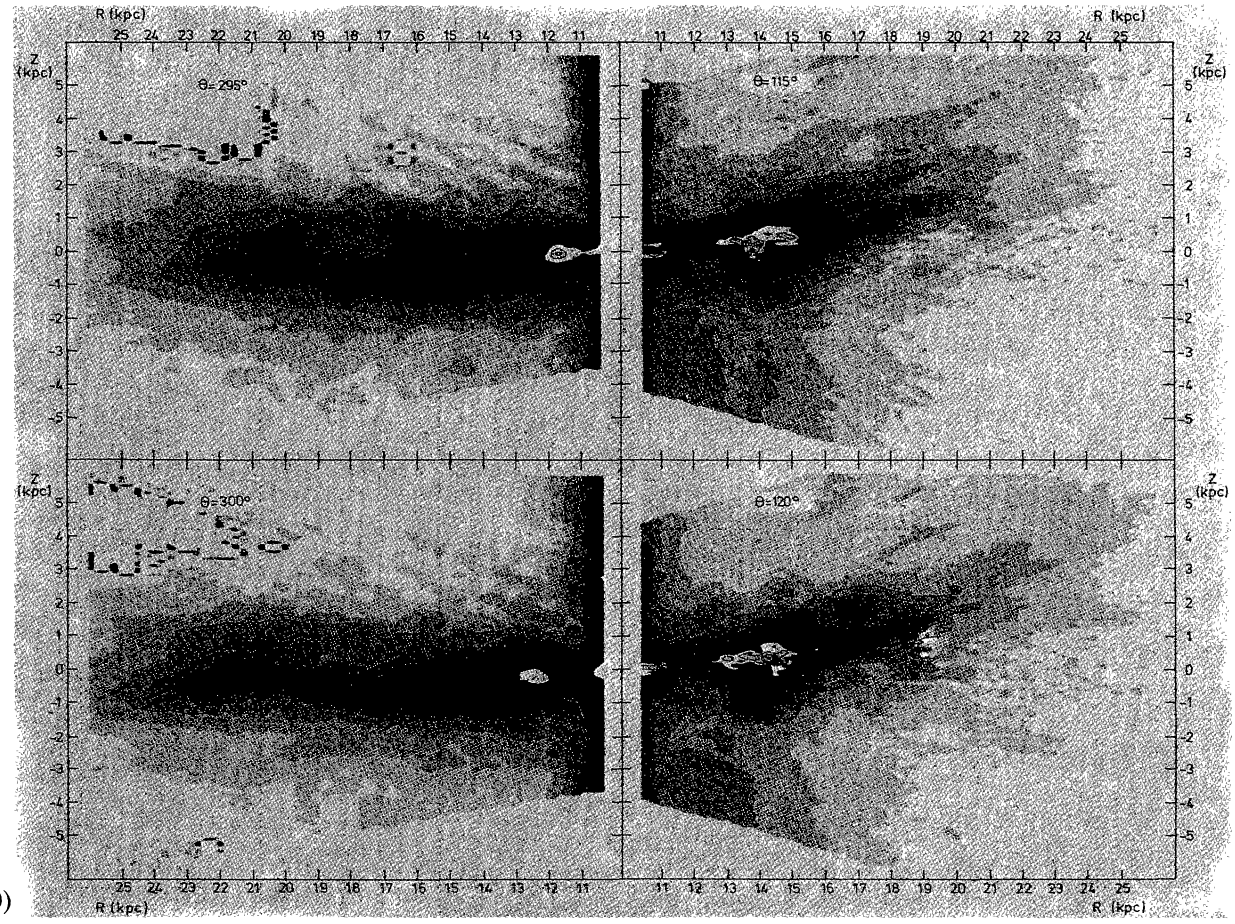

3(10)

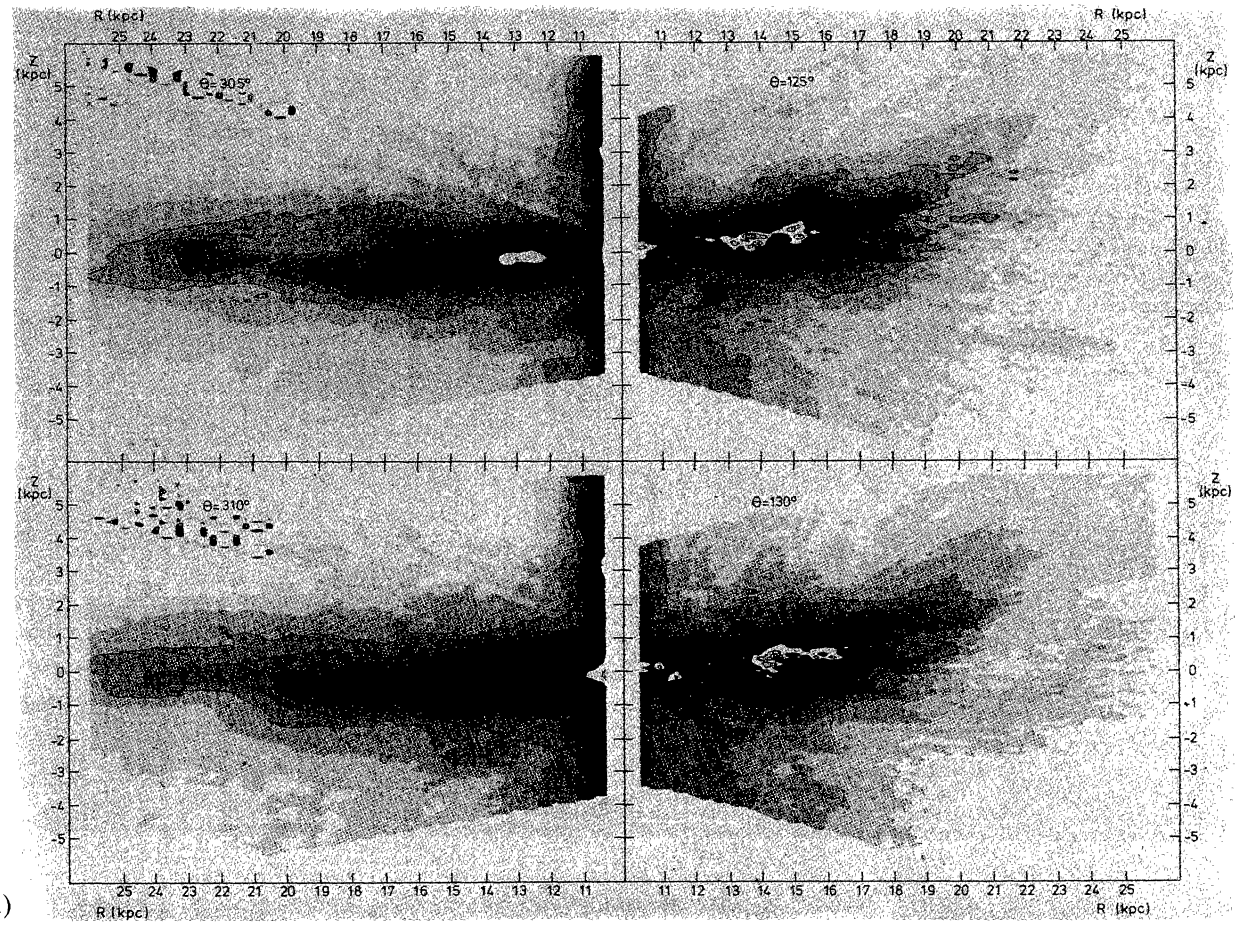

3(11)

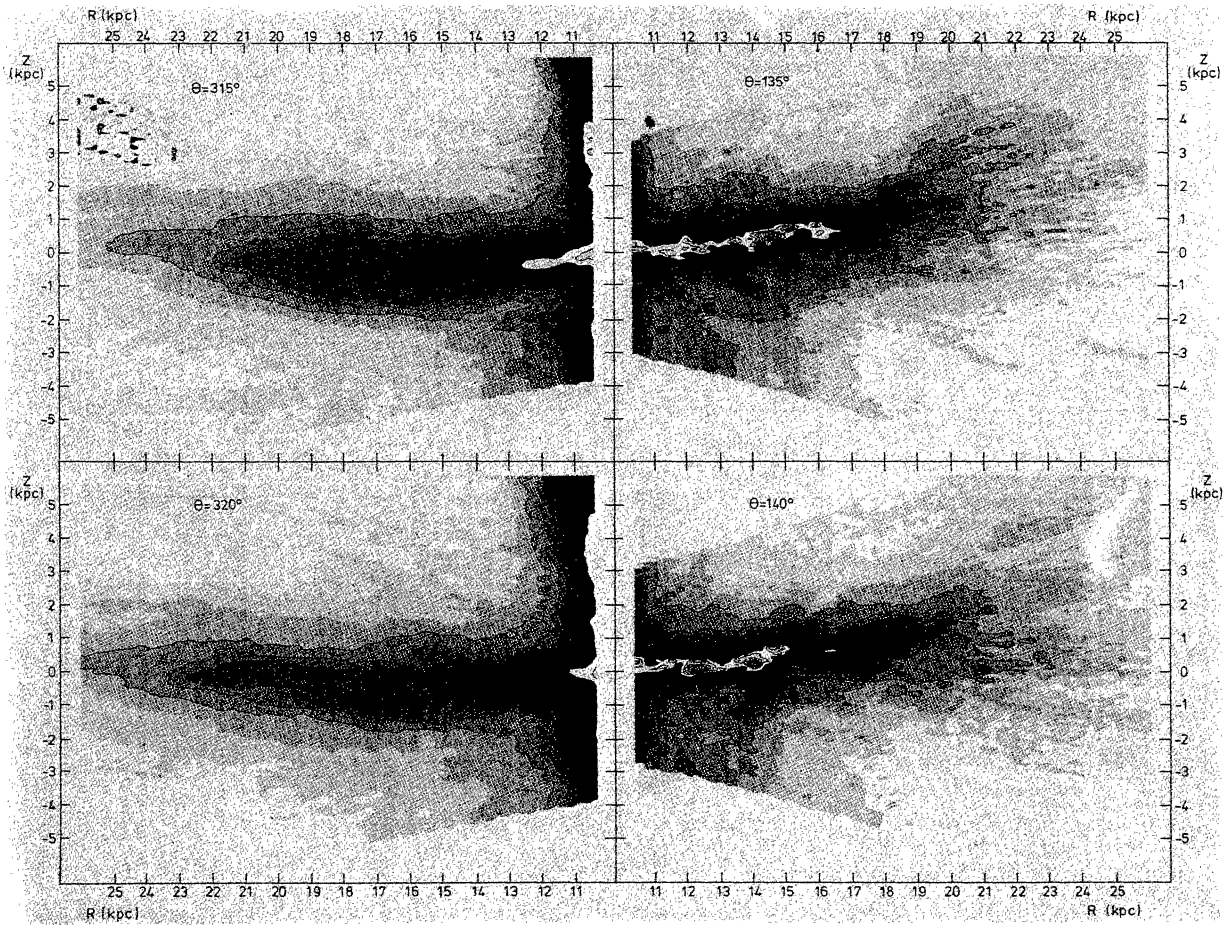

3(12

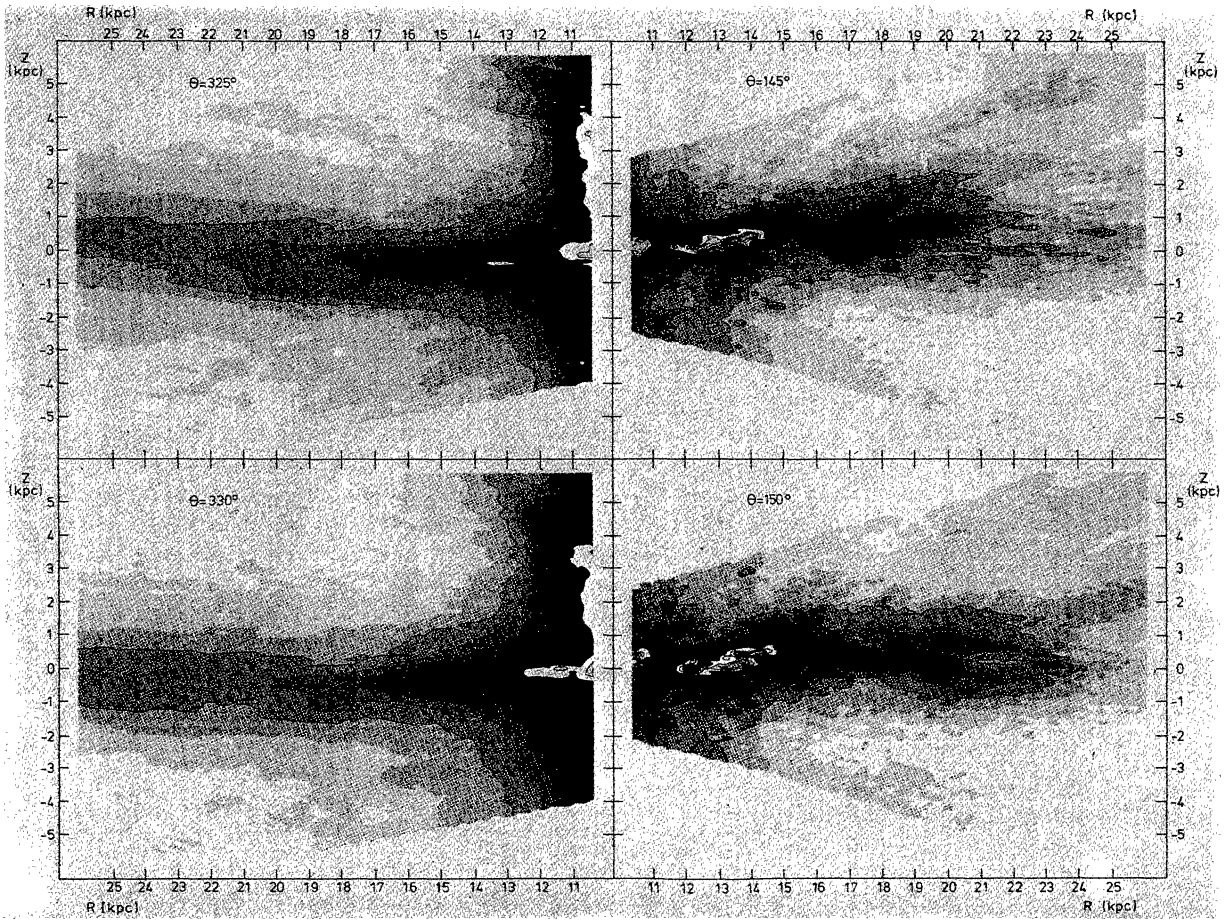

3(13)

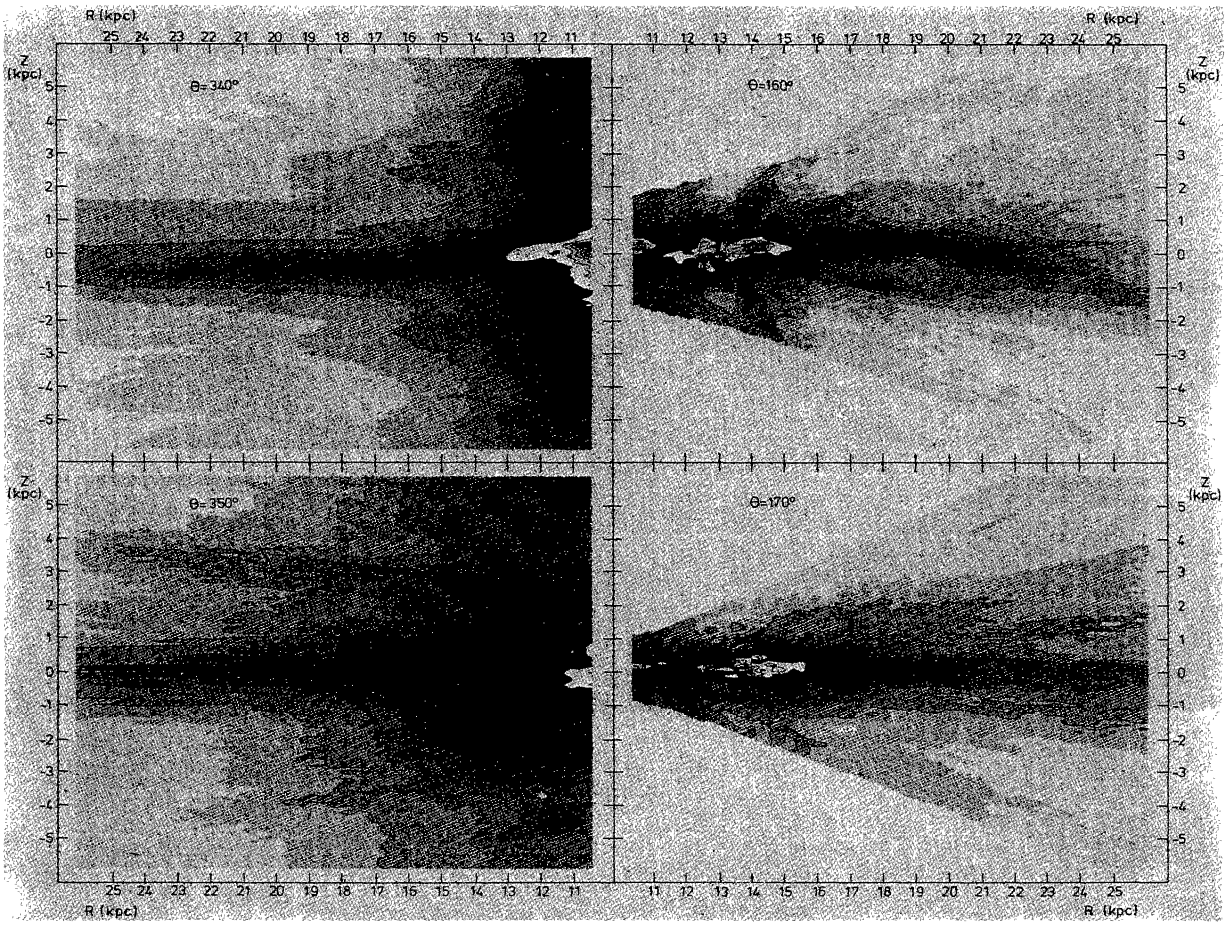

3(14)

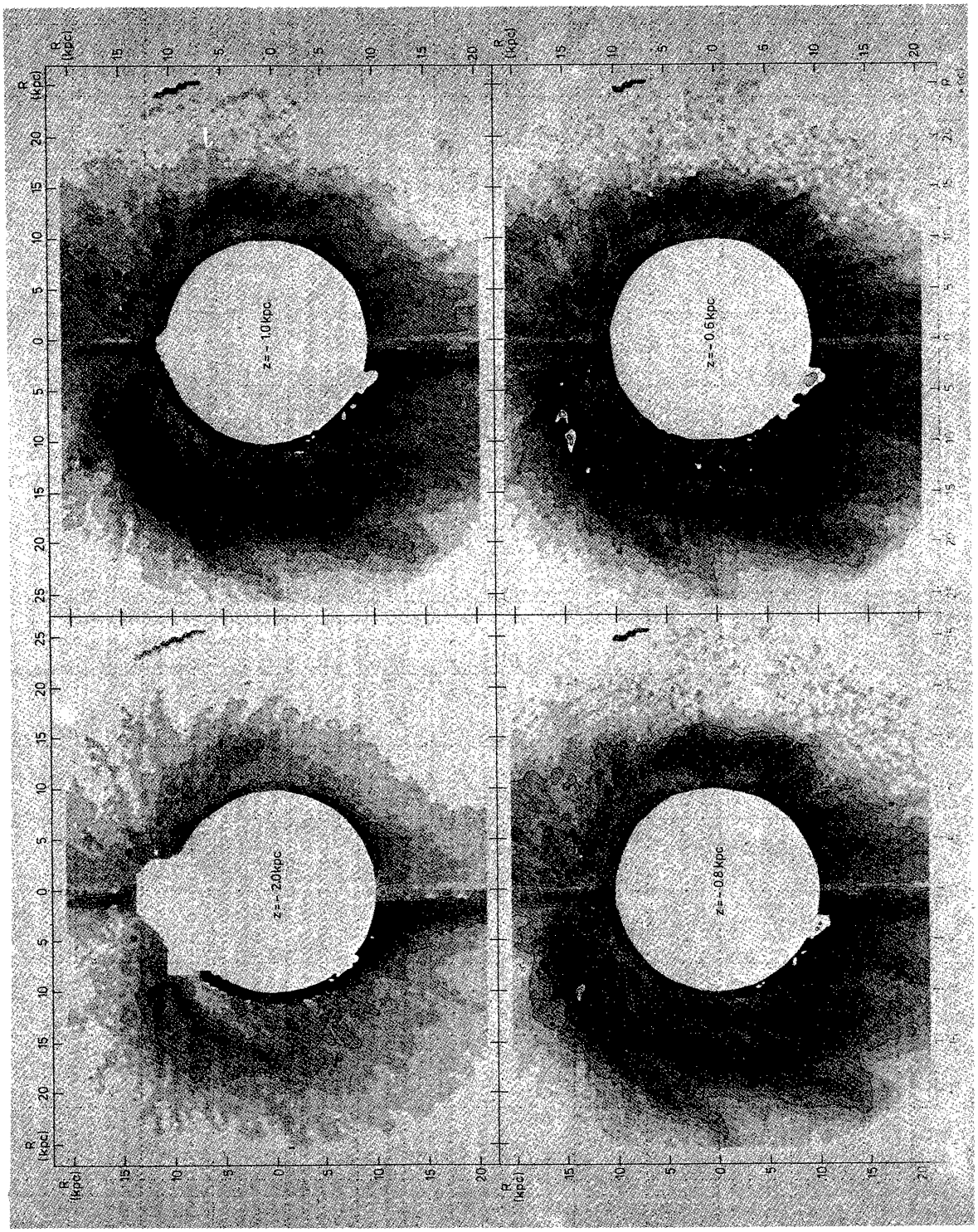

FIGURES 4(1)-4(5). — $R, \theta \mid_z$ maps showing arrangement of hydrogen volume densities in sheets parallel to the galactic equator at the indicated z-heights. Contours and grey-scale levels are drawn at the same values as in figure 1. The cylindrical-coordinate R, θ, z data cube was sampled at 1° intervals in θ and at 250 pc intervals in R ; the range in z-height is ± 50 pc centred on the indicated value.

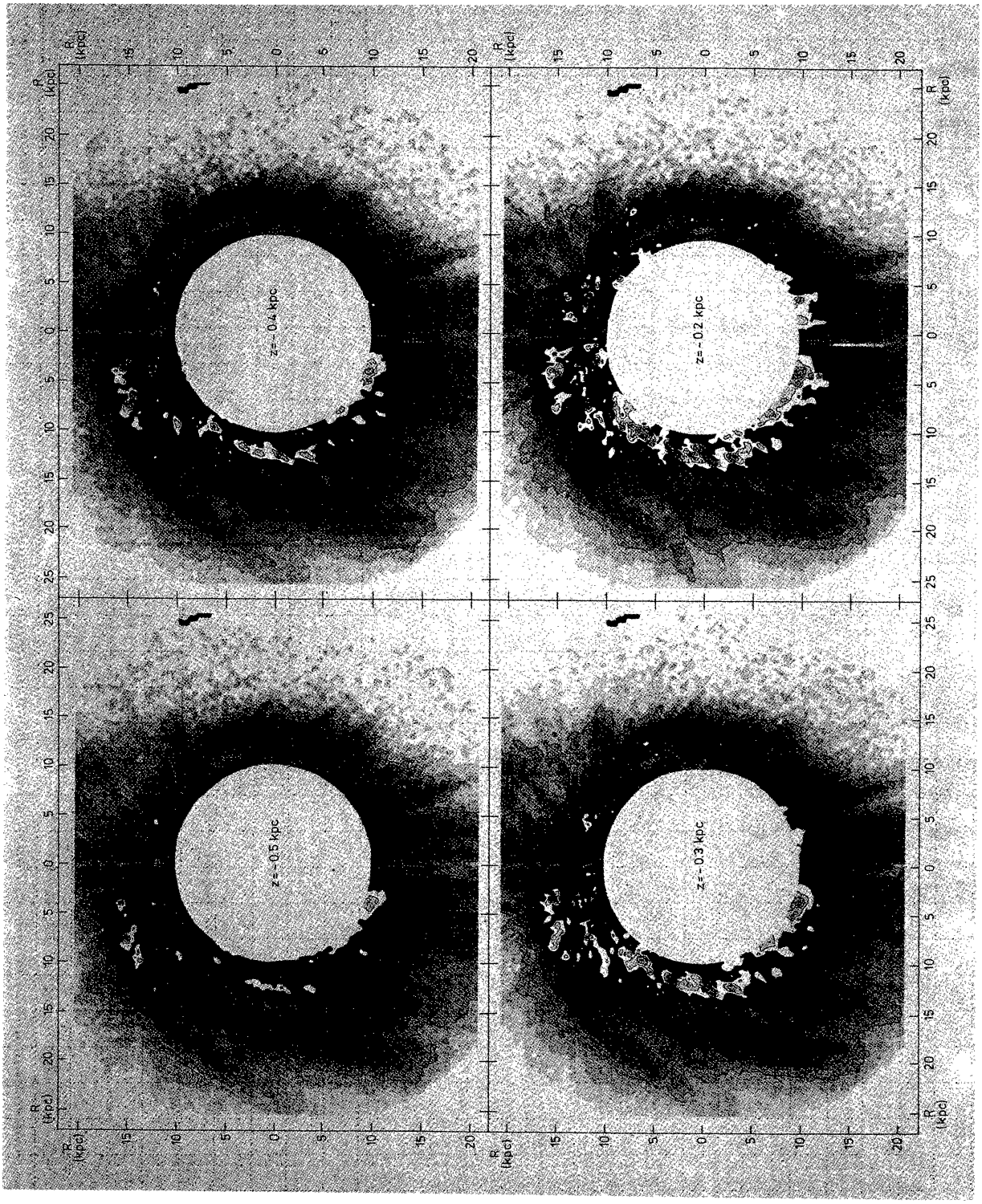

FIGURE 4(2).

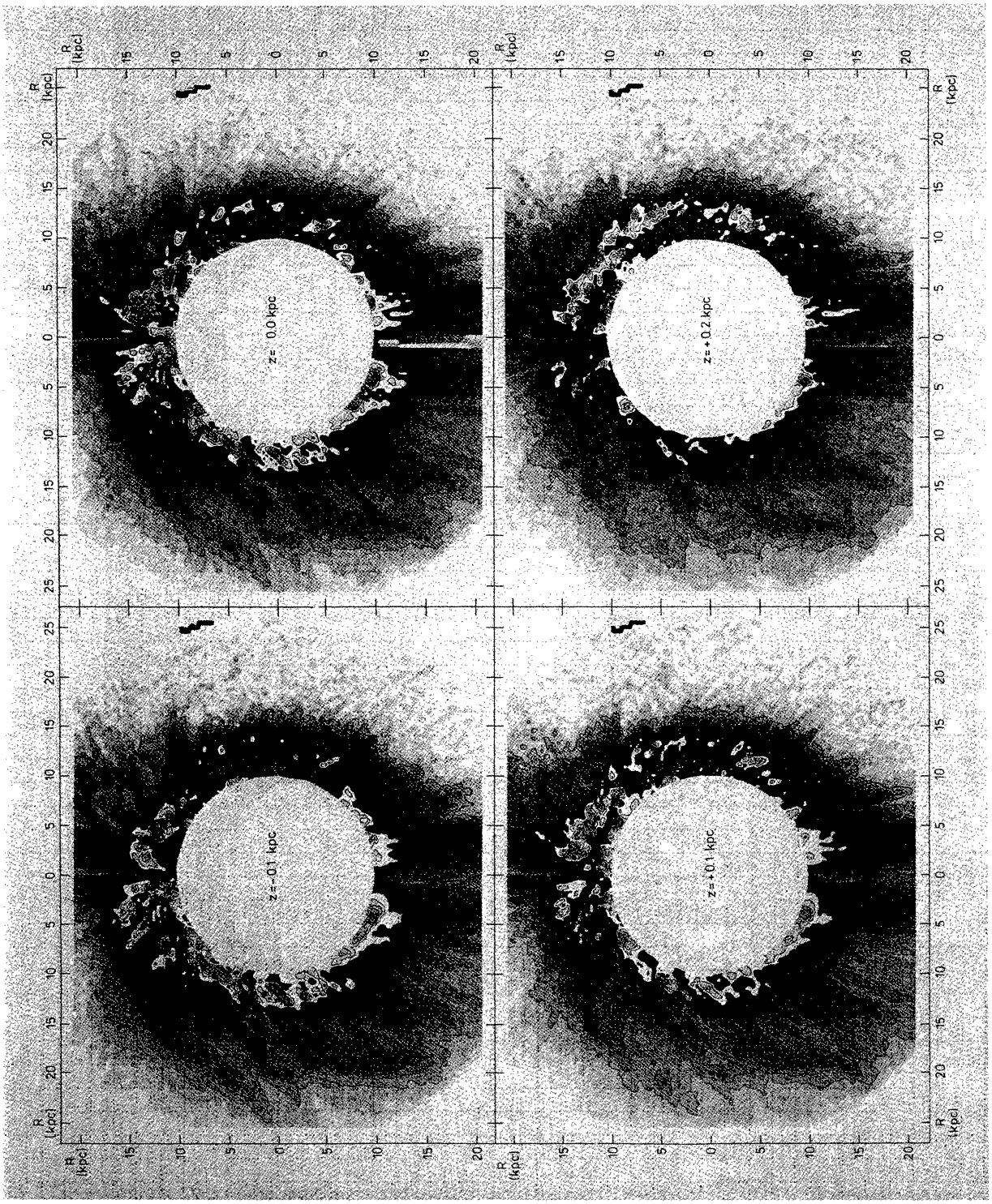

FIGURE 4(3).

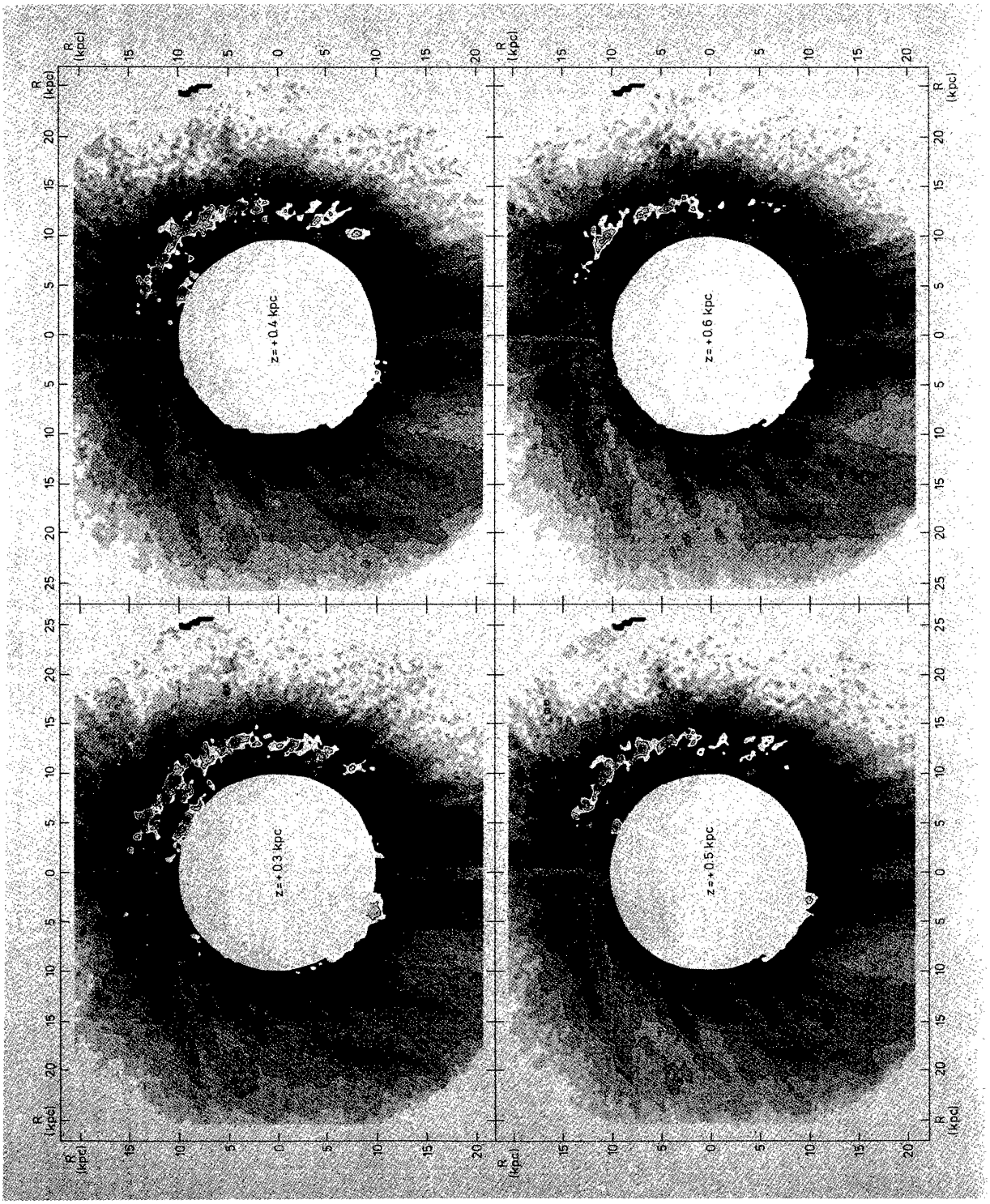

FIGURE 4(4).

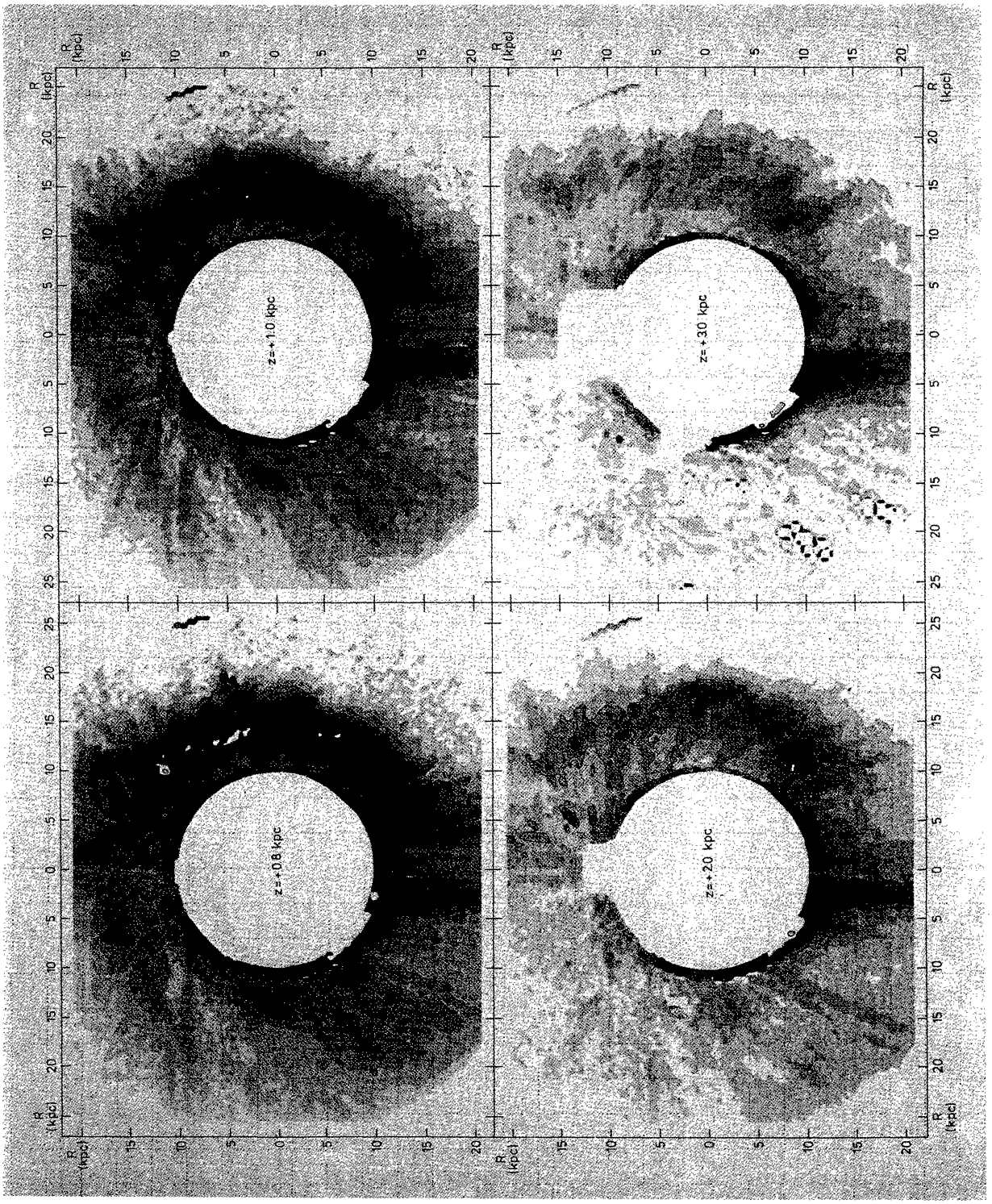

FIGURE 4(5).

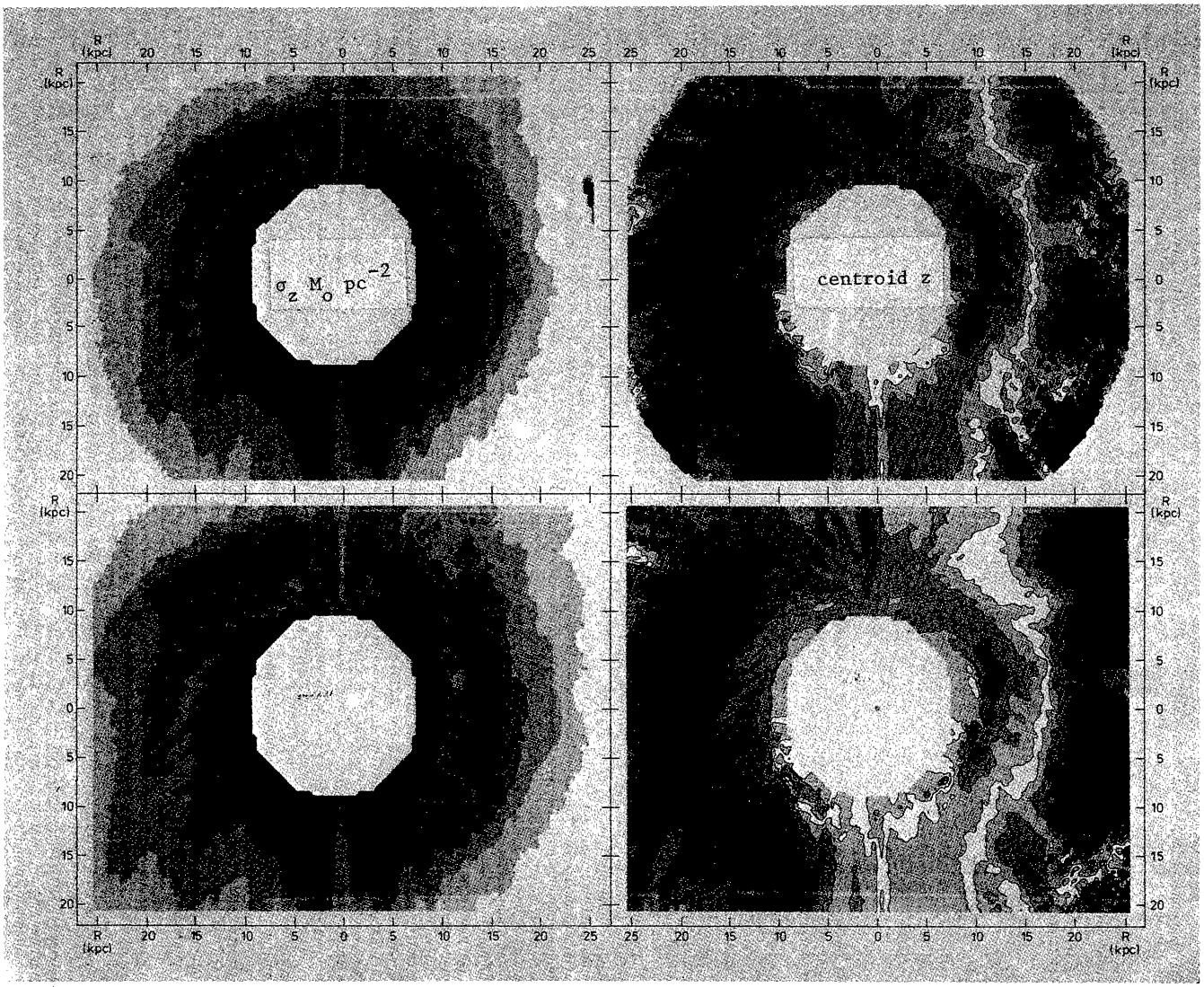

FIGURES 5(1)-5(3). — R, θ maps showing the indicated quantities derived for the case of a flat rotation curve (upper panels) and for the case of a rising one (lower panels). 5(1). — The left panels show the projected HI surface density in units of M_0 pc^{-2}. Contours are drawn at levels of 3, 6, 9, 15, 21, and 48 M_0 pc^{-2}. The right panels show the z-height of the HI mass centroid. Contours are drawn at levels of 0, 150, 450, 750, 1050, 1500, 2000, 3500, and 6000 pc. Grey scale divisions occur at heights where $| z |$ is the same as the contour levels. White is used for $| z | < 150$ pc, $z < -2000$ pc, and $z > 6000$ pc.

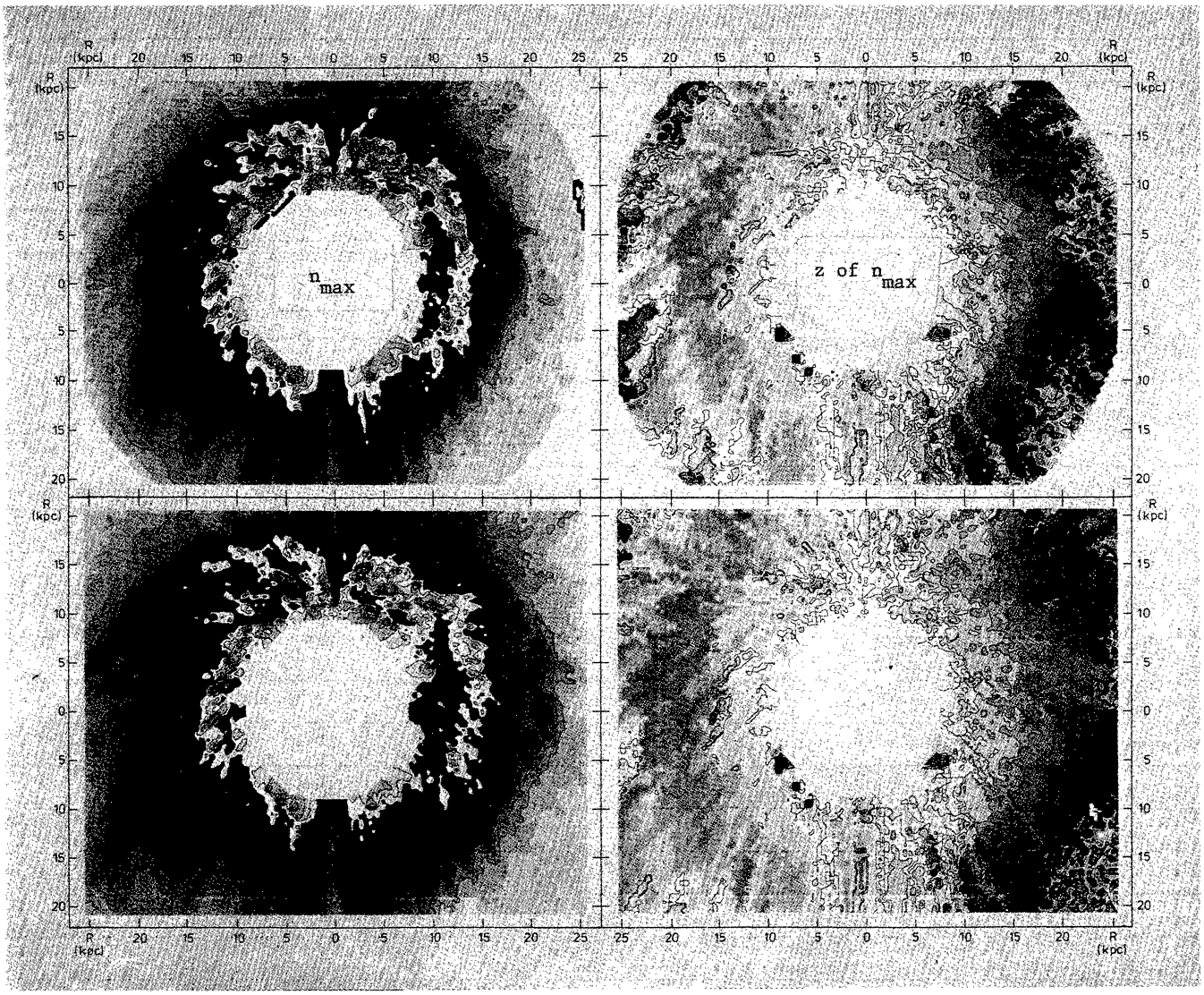

FIGURE 5(2). — The left panels show the maximum value of n_{HI}. Contours and grey-scale levels are drawn at the same values as in figure 2. The right panels show the z-height at which the maximum value of n_{HI} occurs. Contours and grey-scale levels are drawn at the same values as in right panels of figure 5(1).

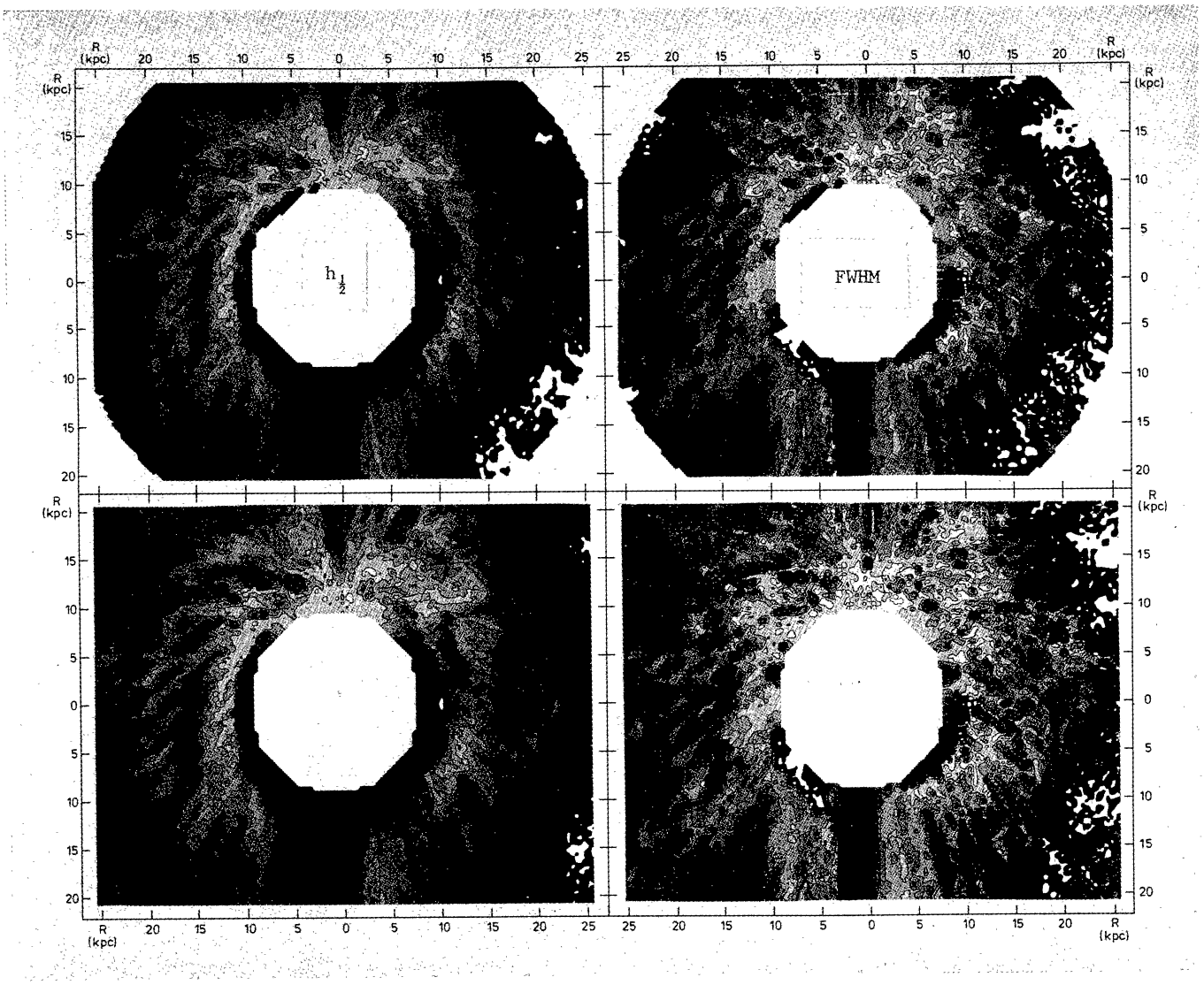

FIGURE 5(3). — The left panels show the thickness of the HI layer containing half the total surface density as measured between heights at which the surface density is one-quarter of its total value. Contours and grey-scale divisions occur at levels of 0, 250, 500, 750, 1000, 1500, 2000, 3500, and 6000 pc. The right panels show, at the same levels, the full-width half-maximum thickness of the HI layer measured between z-heights where the local volume density has dropped to half its maximum value.